SANDIA REPORT

SAND97–2395 • UC–704
Unlimited Release
Printed October 1997

Modeling and Characterization of Molecular Structures in Self Assembled and Langmuir – Blodgett Films for Controlled Fabrication

J. Cesarano III

Prepared by
Sandia National Laboratories
Albuquerque, New Mexico 87185 and Livermore, California 94550

Sandia is a multiprogram laboratory operated by Sandia Corporation, a Lockheed Martin Company, for the United States Department of Energy under Contract DE-AC04-94AL85000.

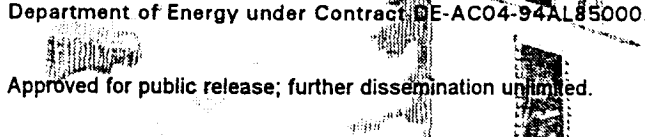

Sandia National Laboratories

SF2900Q(8-81)

Issued by Sandia National Laboratories, operated for the United States Department of Energy by Sandia Corporation.

Available to DOE and DOE contractors from
Office of Scientific and Technical Information
PO Box 62
Oak Ridge, TN 37831

Prices available from (615) 576-8401, FTS 626-8401

Available to the public from
National Technical Information Service
US Department of Commerce
5285 Port Royal Rd
Springfield, VA 22161

NTIS price codes
Printed copy: A08
Microfiche copy: A01

SAND 97-2395 Distribution
Unlimited Release Category UC-704
Printed October 1997

Modeling and Characterization of Molecular Structures in Self Assembled and Langmuir - Blodgett Films for Controlled Fabrication

J. Cesarano III
Materials and Process Sciences Center

Sandia National Laboratories
P. O. Box 5800
Albuquerque, NM 87185-1349

ABSTRACT

Self Assembled (SA) thin films and Langmuir - Blodgett (LB) thin films are emerging technologies for the development of chemical and bio-chemical sensors, electrooptic films, second harmonic generators (frequency doublers), templates for biomimetic growth etc.. However, the growth of these technologies is dependent on the development of our understanding and control of the molecular arrangement of these films. This is not trivial since SA and LB films are essentially two-dimensional monolayer structures. One of the goals of this project was to extend Sandia's characterization techniques and molecular modeling capabilities for these complex two-dimensional geometries with the objective of improving our control of the fabrication of these structures for specific applications. Achieving this requires understanding both the structure throughout the thickness of the films and the in-plane lattice of the amphiphilic molecules. To meet these objectives we used atomic force microscopy (AFM), X-ray reflectivity, and molecular modeling.

While developing these capabilities, three different materials systems were fabricated and characterized: 1) Self Assembled Monolayers (SAMs) of octadecyltrichlorosilane (OTS) and LB films of arachidic acid on silicon wafers; 2) SAMs on PZT substrates; and 3) electrochemical deposition of CdS on LB film templates. The SAMs and LB films deposited on silicon were characterized using characterized using x-ray reflectivity. This technique proved to be useful for understanding the molecularly layered structure in the direction perpendicular to the substrate (see Appendix C). The study of SAMs on PZT was a novel study. The self assembly of OTS has been demonstrated and studied on silica surfaces however, in this work we demonstrated SAM formation on PZT, determined the mechanism for SAM formation on PZT, and demonstrated that SAMs on PZT can modify the surface behavior. These results are discussed in detail in Appendix A and imply that SAMs may be useful for micropatterning of PZT and development of next generation optics-based microelectronics. In Appendix B there is a detailed discussion about using LB films and electrochemistry to create template assisted growth of thin films of CdS. In this work atomic force microscopy was used to characterized the in-plane structure of LB films and to study how the chemical functionality of LB films can effect the growth of CdS.

SUMMARY

Self assembled and Langmuir - Blodgett films have been the focus of intense investigation in recent years. This results from the plethora of possible applications for these unique two-dimensional structures. Applications include chemical and bio-chemical sensors, electrooptic films, second harmonic generators (frequency doublers), and templates for biomimetic growth. However, wide spread use of these films is limited because characterization and control of their two-dimensional geometries has proven evasive. The goal of this research project was to develop a capability for the molecular level characterization, modeling and fabrication of SA and LB films for possible applications in the previously mentioned areas. A farther term objective is to use these new capabilities to improve our control of the fabrication of thin films for specific applications.

The project was completed within three different materials systems and is discussed in detail in Appendices A-C. The project was successful in developing capabilities for fabrication and characterization of self assembled thin film structures in general. However, extensive modeling of the structures proved evasive and is not discussed in detail. The most interesting characterization was completed using atomic force microscopy (AFM) and x-ray reflectivity. The AFM can be used to study local features rather than relying on data averaged over large areas to provide information of molecular ordering. This allows the study of the in-plane structure such as local ordering, defect structures, as well as grain boundaries. X-ray reflectivity can provide detailed structural information throughout the thickness of these films.

Appendix A discusses the formation, characterization, and utility of OTS SAMs on PZT substrates. This is a novel development. Appendix B discusses the fabrication and characterization of CdS thin films that were formed by using LB film templated (i.e., biomimetic) growth in the presence of electric fields. This is another novel development. Finally, the utility of x-ray reflectivity for studying the out-of-plane structure of SAMs and LB films is demonstrated in Appendix C for films deposited on silicon wafers.

In general, the SAMs studied were octadecyltrichlorosilane on silica and hexadecyl mercaptan on gold. The LB films were cadmium arachidate. The following pages highlight the fabrication procedures for the LB films. More detail is provided in the appendices.

Table of Contents

Langmuir Blodgett Films are Highly Ordered Films

- Langmuir-Blodgett films are monolayers or multilayers transferred from the water-air interface onto a solid substrate

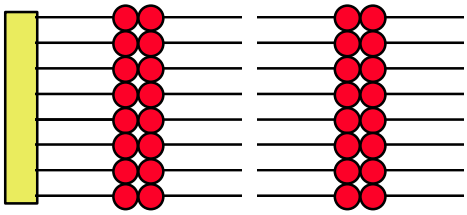

1

Langmuir Films

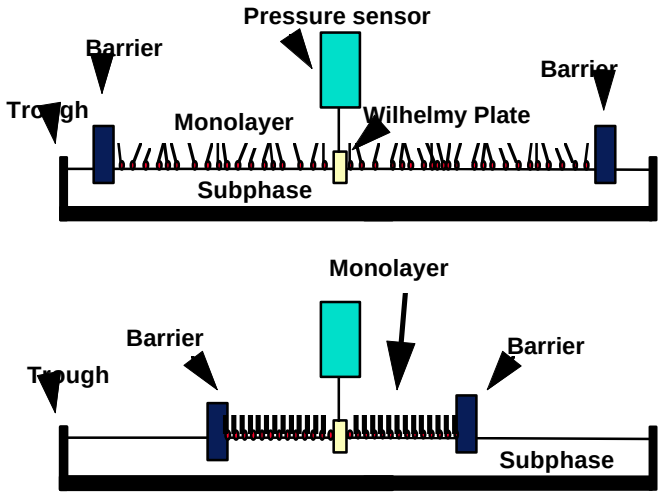

2

LB films Deposited as Substrate Passes Air-water Interface

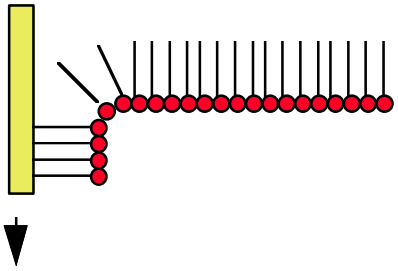

- Hydrophobic substrates begin deposition on first downward pass (Hydrophilic substrates start on first upward pass)
- Hydrophobic tail groups contact substrate and are deposited
- (With hydrophilic substrates, head groups are deposited
- Multilayers are built up “head-to-head and tail-to-tail”

3

Arachidic Acid Used as Deposition Material

- Is an amphiphilic molecule
- Will form ideal LB films

Arachidic Acid

CH_3-$(CH_2)_{18}$-COOH

4

Subphase pH and Cadmium Concentration Control Rigidity of LB Film

- Higher pH and concentration of Cd^{+2} ions in subphase form more rigid monolayers
- Less acidic pH promotes dissociation of carboxylic group

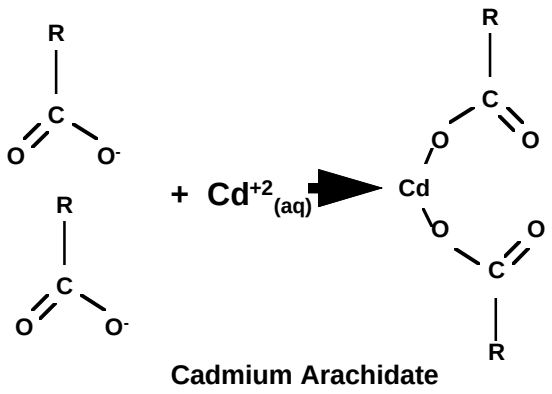

Cadmium Arachidate

5

Substrates Treated to Form Hydrophobic Surface

- Silicon wafers and PZT substrates treated with Octadecyltrichlorosilane(OTS),
- Methyl terminated chain makes substrate surface hydrophobic
- Hexadecyl Mercaptan, $HS - (CH_2)_{15} - CH_3$, reacts in a similar way with gold coated wafers

6

Chemical Functionality of 4 and 5 layer LB Films

- Four layer films have the methyl group outward

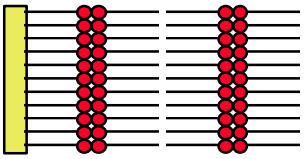

—— = -CH_3

- Five layer films have carboxylic acid group outward

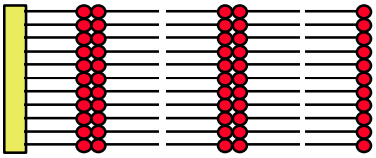

● = -COO^-

7

Conditions Used for Biomimetic Templating

- Biomimetic template processing imitates the deposition of inorganics on an organic layer
- Previous trials led to the following conditions:
  - pH : 6.5
  - [Cd^{+2}] : 5 x 10^{-4}M

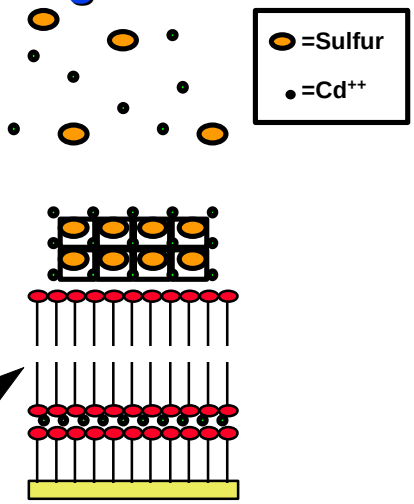

8

APPENDIX A

Formation and Stability of Self-Assembled Monolayers on Thin Films of Lead Zirconate Titanate (PZT)

Rajesh Vaidya, R. J. Simonson, Joseph Cesarano III, Duane Dimos, and Gariel Lopez

Center for Micro-Engineered Ceramics, Department of Chemical and Nuclear Engineering, University of New Mexico, Albuquerque, New Mexico 87131, and Materials and Process Sciences Center, Sandia National laboratories, Albuquerque, New Mexico 87185-5800

Published in: *Langmuir* **1996,** *12,* 2830 - 2836

Sandia is a multiprogram laboratory operated by Sandia Corporation, a Lockheed Martin Company, for the United States Department of Energy under Contract DE-AC04-94AL85000.

Formation and Stability of Self-Assembled Monolayers on Thin Films of Lead Zirconate Titanate (PZT)

Rajesh Vaidya,[†] R. J. Simonson,[‡] Joseph Cesarano III,[‡] Duane Dimos,[‡] and Gabriel P. López*,[†]

Center for Micro-Engineered Ceramics, Department of Chemical and Nuclear Engineering, University of New Mexico, Albuquerque, New Mexico 87131, and Sandia National Laboratories, Advanced Materials Laboratory, 1001 University Boulevard, Albuquerque, New Mexico 87106

Received November 27, 1995[⊗]

Self-assembled monolayers (SAMs) of alkylsiloxanes were formed from hexyltrichlorosilane (HTS) and octadecyltrichlorosilane (OTS) on surfaces of thin films of a complex oxide, lead zirconate titanate (PZT). X-ray photoelectron spectroscopy (XPS) and contact angle measurements confirmed the formation of a thin, uniform organic layer on the surface of the PZT, consistent with the hypothesis that a densely packed organic monolayer is formed on the PZT. Angle-resolved high-resolution XPS suggested that the surface of the PZT thin film includes a top layer deficient in titanium and consisting mainly of oxides of lead and zirconium, along with hydroxylated zirconium that may react with alkyltrichlorosilanes to form the SAMs. The effect on these SAMs of exposure to acidic media was probed by wettability measurements, XPS, and scanning electron microscopy (SEM). Contact angle measurements with water and hexadecane indicated that the SAMs formed from the longer alkylsilane, OTS, were stable in HCl over long periods of time (at least 3 days), while the SAMs formed from the short-chain alkylsilane, HTS, degraded after 12 h. The XPS spectra of SAMs formed from OTS and exposed to HCl solution were similar to those obtained for similar SAMs not exposed to HCl. SEM also confirmed that the SAMs formed from OTS can act as protective barriers for PZT against etching by HCl.

Introduction

The search for new materials for applications in the next generation of optics-based microelectronics has resulted in the development of many oxide materials with unique properties. Many complex oxides (e.g., dielectrics such as $PbTiO_3$, $BaTiO_3$, and $Pb(Zr,Ti)O_3$ and electrodes such as RuO_2 and In_2O_3 + SnO_2, ITO) are receiving increased attention due to their distinctive electrical, magnetic, optical, thermal, and mechanical properties and the potential for their integration into optoelectronic devices, such as nonvolatile memories.[1-5] We are interested in the fabrication by sol-gel routes of thin films of various oxides including silica, titania, zirconia, and, in particular, lead zirconate titanate (PZT). PZT ceramic thin films have been under extensive scrutiny because of their excellent optoelectronic,[6-8] piezoelectric,[3] and ferroelectric[1] properties. They have been proposed for applications in nondestructive memory readout,[1,7-9] as capacitors,[10,11] as optical waveguides,[12] and as ultrasonic transducers and microactuators.[3] These oxides, however, are susceptible to chemical degradation during the numerous processing steps comprising the fabrication of dense, integrated, optoelectronic circuits; for example, PZT is slowly etched in even slightly acidic solutions. In this paper, we demonstrate that, by forming self-assembled monolayers of alkylsiloxanes on their surfaces, it is possible to modify the surface chemistry of complex oxide materials (namely, PZT). Consequently, alkylsilanes can be chosen such that SAMs formed from them will modify the surface of the PZT to control interfacial properties and hence control adhesion, minimize contamination, or participate in molecular recognition events. Furthermore, thin films of PZT can be stabilized toward etching in acidic conditions over a wide range of pH values.

Much of the interest in self-assembly of such molecules as alkanethiols on the surface of coinage metals[13-20] and semiconductors,[21-23] and alkylchlorosilanes on oxidized substrata[13,24-29] such as silica and alumina is derived from the recognition that these systems can be used not only

* Author to whom correspondence should be addressed. Telephone: (505) 277- 4939. Fax: (505) 277-5433. E-mail: gplopez@unm.edu.

[†] University of New Mexico.

[‡] Sandia National Laboratories.

[⊗] Abstract published in *Advance ACS Abstracts,* May 1, 1996.

(1) Geideman, W. A. *IEEE Trans. Ultrason., Ferroelect., Freq. Control* **1991**, *38*, 704–711.
(2) Sayer, M.; Sreenivas, K. *Science* **1990**, *247*, 1056–1060.
(3) Sayer, M.; Barrow, D.; Zou, L.; Kumar, C. V. R. V.; Noteboon, B.; Knapik, D. A.; Schnidel, D. W.; Hutchins, D. A. *Mater. Res. Soc. Symp. Proc.* **1993**, *310*, 37–46.
(4) Sanchez, L. E.; Wu, S.; Naik, I. K. *Appl. Phys. Lett.* **1990**, *56*, 2399.
(5) Okahata, Y.; Yokobori, M.; Ebara, Y.; Eboto, H.; Ariga, K. *Langmuir* **1990**, *6*, 1148.
(6) Dimos, D. *Annu. Rev. Mater. Sci.* **1995**, *25*, 273.
(7) Thakoor, S. *Appl. Phys. Lett.* **1992**, *60*, 3319–3321.
(8) Thakoor, S. *Appl. Phys. Lett.* **1993**, *63*, 3233–3235.
(9) Afanasjev, V. P.; Kramar, G. P. *Ferroelectrics* **1993**, *143*, 299–304.
(10) Teowee, G.; Uhimann, D. R. *Mater. Res. Soc. Symp. Proc.* **1993**, *310*, 415–422.
(11) Patel, A.; Logan, E. A.; Nicklin, R.; Hasdell, N. B.; Whatmore, R. W.; Uren, M. *Mater. Res. Soc. Symp. Proc.* **1993**, *310*, 447–452.
(12) Wood, V. E.; Busch, J. R.; Ramamurthi, S. D.; Swartz, S. L. *J. Appl. Phys.* **1992**, *71*, 4557–4566.
(13) Ulman, A. *An Introduction to Ultrathin Organic Films from Langmuir–Blodgett to Self-Assembly*; Academic Press Inc.: San Diego, CA, 1991.
(14) Dubois, L. H.; Nuzzo, R. G. *Annu. Rev. Phys. Chem.* **1992**, *43*, 437.
(15) Chidsey, C. E. D.; Porter, M. D.; Allara, D. L. *J. Electrochem. Soc.* **1986**, *133*, 130.
(16) Bain, C. D.; Whitesides, G. M. *Adv. Mater.* **1989**, *1*, 110.
(17) Whitesides, G. M.; Laibinis, P. E. *Langmuir* **1990**, *6*, 87–96.
(18) Chidsey, C. E. D.; Loicano, D. N. *Langmuir* **1990**, *6*, 682.
(19) Nuzzo, R. G.; Allara, D. L. *J. Am. Chem. Soc.* **1983**, *105*, 4481–4483.
(20) Troughton, E. B.; Bain, C. D.; Whitesides, G. M.; Nuzzo, R. G.; Allara, D. L.; Porter, M. D. *Langmuir* **1988**, *4*, 365–385.
(21) Lunt, S. R.; Santagangelo, P. G.; Lewis, N. S. *J. Vac. Sci. Technol.* **1991**, *B9*, 2333–2336.
(22) Nakagawa, O. S.; Ashok, S.; Sheen, C. W.; Martensson, J.; Allara, D. L. *Jpn. J. Appl. Phys.* **1991**, *30*, 3759–3762.
(23) Sheen, C. W.; Shi, J.-X.; Martensson, J.; Parikh, A. N.; Allara, D. L. *J. Am. Chem. Soc.* **1992**, *114*, 1514–1515.
(24) Sagiv, J. *J. Am. Chem. Soc.* **1980**, *102*, 92–98.

to generate model surfaces for the study of a variety of phenomena including wetting,[30-33] adhesion,[34-36] molecular recognition,[37] and interactions of biological systems with synthetic materials[34,36,38] but also as barrier layers and ultrathin resists.[20,39-42] Self-assembled monolayers (SAMs) formed from alkyltrichlorosilanes on silica have been studied using numerous techniques including wettability measurements,[28,30] ellipsometry,[28,29] X-ray reflectivity,[29,43] X-ray photoelectron spectroscopy (XPS),[28,44,45] and Fourier transform infrared (FTIR) spectroscopy.[43,46-48] These studies have shown that SAMs formed from alkyltrichlorosilanes (e.g., octadecyltrichlorosilane, OTS) on silica tend to be fully hydrolyzed, hydrophobic, well-ordered assemblies in which the aliphatic chains tend to be extended in an all-trans configuration.

In the present work, it was our hypothesis that stable, uniform monolayers can be formed from alkylchlorosilanes on the disordered surface of multicomponent oxide materials and that SAMs can be used to modify the surface of these oxides to yield surfaces with low free energy and to act as effective barriers against etching by commonly used acids, such as HCl, that are known to dissolve these oxides. We tested this hypothesis in several ways: we formed monolayers on thin films of the oxide PZT by self-assembly of short- and long-chain alkyltrichlorosilanes and subjected them to strong solutions of HCl for various periods of time. We then probed their wettability and composition by contact angle measurements and XPS, respectively. We also used scanning electron microscopy (SEM) to illustrate the effect of exposure to HCl of the PZT thin films and of PZT thin films upon which SAMs of OTS have been formed.

Experimental Section

Hexyltrichlorosilane ($Cl_3Si(CH_2)_5CH_3$, HTS) and octadecyltrichlorosilane ($Cl_3Si(CH_2)_{17}CH_3$, OTS) were obtained from United Chemical Technologies, Inc., Bristol, PA, and distilled under vacuum. Dry hexadecane was obtained from Aldrich in Aldrich SureSeal bottles. All other solvents and chemicals used were of reagent grade. The thin films (~4000 Å thick) of PZT with a nominal composition of $PbZr_{0.4}Ti_{0.6}O_3$ were formed by a sol-gel spin-coating process as described elsewhere.[49-51] The PZT was coated on a Pt layer (~3500 Å thick) sputter-deposited on SiO_2 (~3500 Å thick, thermally grown on the Si wafer) with ~500 Å of Ti as an adhesion layer between SiO_2 and Pt. These were fired at 650 °C for 30 min (ramp rate 50 °C/min) to obtain the ferroelectric perovskite phase.[49,50] The PZT substrates were cleaned in an air plasma at 0.25 Torr, 35 W radio frequency power for 2 min. For comparison, SAMs were also formed on silicon wafers with a 15 Å thick native oxide layer (as determined by ellipsometry). The silicon wafers were cleaned in a solution of sulfuric acid and hydrogen peroxide in the ratio 7:3 (piranha solution) and rinsed with copious amounts of deionized water.[28] *Caution: piranha solution is a very strong oxidant and should be handled with care.* We also used Si/SiO_2 substrates cleaned in a radio frequency plasma using the same procedure as for PZT. Both the Si/SiO_2 and PZT substrates were stored in deionized water immediately after cleaning until used in the silanation reactions (typically for less than 15 min).

All silanation reactions were carried out in glass vials cleaned in piranha solution, rinsed copiously with deionized water, and dried at 150 °C in an oven. The reactions were carried out in a glovebox filled with dry nitrogen. Dry hexadecane was first transferred from an Aldrich SureSeal bottle into the vial, and an appropriate amount of distilled alkyltrichlorosilane (HTS or OTS) was then added to the vial to make a 1 mM solution of the silane. The clean substrates (Si/SiO_2 or PZT) were rinsed with deionized water, dried in a stream of nitrogen or argon, and quickly transferred to the glovebox. The substrates were placed in the solutions of HTS or OTS for 12 h. At the end of this period, the substrates were transferred to another vial containing dry hexadecane, removed from the glovebox, sonicated for 5 min to remove excess silane, and rinsed thoroughly with carbon tetrachloride and ethanol. To monitor the etching of PZT thin films by HCl, experiments were carried out by placing the plasma-cleaned PZT samples and samples of PZT with the SAM overlayer in a mildly stirred (~60 rpm) solution of HCl. The samples were removed sequentially from HCl, rinsed with water, and dried in a stream of N_2 or Ar.

All contact angles of water and hexadecane on SAMs were obtained using a VCA2000 contact angle goniometer within 15 min after removal from the silanation solutions.[28] At least three measurements of the advancing and receding contact angles were obtained for each sample and averaged (standard deviation for each reported value $<\pm 2°$). All ellipsometric thickness measurements were performed within 5 min of removal of the samples from silanation solutions using a Gaertner L116C ellipsometer equipped with a He-Ne laser (λ = 6328 Å) light source. The angle of incidence was 70° and the compensator was set at −45°. A refractive index of 1.45 was assumed for the SAM overlayer.[28]

X-ray photoelectron spectra were obtained from the same samples for which contact angles and ellipsometric thicknesses were measured, using a Physical Electronics 5400 ESCA system with a chamber base pressure of $<1 \times 10^{-9}$ Torr. The spectra were obtained within two days after removal of the samples from the solutions of silanes. XPS data were acquired using monochromatized Al Kα radiation at two takeoff angles, 24° and 68°. *The takeoff angles were measured from the plane of the surface to the detector, so that at the smaller angle, XPS is more surface-sensitive than at the larger one.* The total power applied to the Al Kα X-ray source was 400 W. Monitoring of the C 1s peak intensity relative to the PZT substrate peaks as a function of the total X-ray irradiation time for a given area on the OTS-covered samples indicated that measurable irradiation-induced desorption occurred for this system. In order to minimize this effect, spectra of the OTS-covered substrates were acquired from a "fresh" (i.e., not previously irradiated) area each time, and the spectral acquisition times were kept to minimum amounts consistent with required signal-to-noise (typically ~20 min). On the basis of extrapolation from a series of repeated measurements

(25) Allara, D. L.; Nuzzo, R. G. *Langmuir* **1985**, *1*, 45–52.
(26) Allara, D. L.; Nuzzo, R. G. *Langmuir* **1985**, *1*, 52–66.
(27) Ulman, A. *Adv. Mater.* **1990**, *2*, 573–582.
(28) Wasserman, S. R.; Tao, Y.; Whitesides, G. M. *Langmuir* **1989**, *5*, 1074–1087.
(29) Wasserman, S. R.; Whitesides, G. M.; Tidswell, I. M.; Ocko, B. M.; Pershan, P. S.; Axe, J. D. *J. Am. Chem. Soc.* **1989**, *111*, 5852.
(30) Bain, C. D.; Whitesides, G. M. *J. Am. Chem. Soc.* **1988**, *110*, 5897.
(31) Dubois, L. H.; Zegarski, B. R.; Nuzzo, R. G. *J. Am. Chem. Soc.* **1990**, *112*, 570–579.
(32) Abbott, N. L.; Whitesides, G. M. *Langmuir* **1994**, *10*, 1493.
(33) Lopez, G. P.; Biebuyck, H. A.; Whitesides, G. M. *Science* **1993**, *260*, 647–649.
(34) Prime, K. L.; Whitesides, G. M. *Science* **1991**, *252*, 1164–1167.
(35) Pale-Grosdemange, C.; Simon, E. S.; Prime, K. L.; Whitesides, G. M. *J. Am. Chem. Soc.* **1991**, *113*, 12–20.
(36) Lopez, G. P.; Albers, M. W.; Schreiber, S. L.; Carroll, R.; Peralta, E.; Whitesides, G. M. *J. Am. Chem. Soc.* **1993**, *115*, 5877–5878.
(37) Häussling, L.; Ringsdorf, H.; Schmitt, F.-J.; Knoll, W. *Langmuir* **1991**, *7*, 1837–40.
(38) Lopez, G. P.; Biebuyck, H. A.; Haerter, R.; Kumar, A.; Whitesides, G. M. *J. Am. Chem. Soc.* **1993**, *115*, 10774–10781.
(39) Maoz, R.; Sagiv, J. *Thin Solid Films* **1985**, *132*, 135.
(40) Maoz, R.; Sagiv, J. *Langmuir* **1987**, *3*, 1034.
(41) Maoz, R.; Sagiv, J. *Langmuir* **1987**, *3*, 1045.
(42) Lercel, M. J.; Redinbo, G. F.; Allara, D. L. *Appl. Phys. Lett.* **1994**, *65*, 974.
(43) Porter, M. D.; Bright, T. B.; Allara, D. L.; Chidsey, C. E. D. *J. Am. Chem. Soc.* **1987**, *109*, 3559–3568.
(44) Offord, D. A.; Griffin, J. H. *Langmuir* **1993**, *9*, 3015–3025.
(45) Laibinis, P. E.; Bain, C. D.; Whitesides, G. M. *J. Phys. Chem.* **1991**, *95*, 7017.
(46) Nuzzo, R. G.; Zegarski, B. R.; Dubois, L. H. *J. Am. Chem. Soc.* **1987**, *109*, 733.
(47) Cheng, S. S.; Scherson, D. A.; Sukenik, C. N. *J. Am. Chem. Soc.* **1992**, *114*, 5436.
(48) Tripp, C. P.; Hair, M. L. *Langmuir* **1995**, *11*, 1215–1219.
(49) Schwartz, R. W.; Bunker, B. C.; Dimos, D. B.; Assink, R. A.; Tuttle, B. A.; Tallant, D. R.; Weinstock, I. A. *Int. Ferroelectrics* **1992**, *2*, 243.
(50) Assink, R. A.; Schwartz, R. W. *Chem. Mater.* **1993**, *5*, 511.
(51) Brinker, C. J.; Scherer, G. W. *Sol-Gel Science: The Physics and Chemistry of Sol-Gel Processing*; Academic Press: San Diego, CA, 1990.

on a single area of an OTS-covered PZT substrate, the attenuation of the C 1s signal relative to the substrate signals during a single spectral acquisition was on the order of 10–15%. Survey spectra (1 scan for each sample, shown in Figure 2) were acquired using a pass energy of 89.45 eV, constant analyzer energy resolution $\Delta E = 1.34$ eV, and a spot size of 1 mm^2. For the higher resolution spectra (presented in Figures 3–6), the analyzer pass energy was 35.75 eV with a resolution $\Delta E = 0.54$ eV. The high-resolution spectra were normalized such that the highest peaks in all the spectra presented in Figures 3–6 were of similar height. The peaks were referenced to the C 1s peak at 284.6 eV for charge correction. For quantitation of individual elements in the SAMs and the substrate, we used the Si 2p (for Si/SiO_2 samples), Ti 2p, Pb 4f, and Zr 3d (for PZT samples), along with the O 1s and C 1s photoelectron peaks. The curve fits for the high-resolution spectra in Figures 5 and 6 were generated by subtraction of a Shirley background,[52] followed by nonlinear least-squares fitting of a pair of Zr 3d doublets. Both doublets were constrained to a $3d_{3/2}$–$3d_{5/2}$ binding energy splitting of 2.4 eV, with relative $3d_{3/2}$:$3d_{5/2}$ intensities of 2:3.[53]

SEM was carried out in the secondary electron detection mode of a Hitachi S800 scanning electron microscope (10 keV primary electron beam, chamber pressure ~10^{-7} Torr).

Results and Discussion

We determined the thickness of SAMs formed on Si/SiO_2 substrates by ellipsometry. The thicknesses of the SAMs of HTS and OTS on Si/SiO_2 were 10 ± 2 and 26 ± 1 Å, respectively,[54] consistent with the thickness expected for a densely packed monolayer with alkyl chains oriented perpendicular to the substrate in an all-trans configuration.[28] Ellipsometric measurements are reported only for the Si/SiO_2 samples, since, for PZT samples, the error in measured thickness of the SAM was on the order of the thickness of the SAM itself (±30 Å) due to the roughness of the PZT surface.[55] However, in light of the XPS data presented below, we infer that the thicknesses of SAMs formed from HTS and OTS on the surface of PZT were approximately equal to the thickness of similar SAMs formed on Si/SiO_2.

We investigated the stability of SAMs formed from HTS (a short-chain alkylsilane) and OTS (a long-chain alkylsilane) on Si/SiO_2 and PZT by measurement of wettability, X-ray photoelectron spectroscopy (XPS), and scanning electron microscopy (SEM). Figure 1A presents the results of wettability measurements conducted on SAMs formed from HTS and OTS on PZT and placed in solutions of HCl with pH ranging from 1 to 7 for 2 h. The advancing and receding contact angles of water for SAMs formed from HTS on both PZT and Si/SiO_2 substrates were 107° and 95°, respectively; for SAMs formed from OTS, these values were 113° and 102°, respectively (the contact angles reported here are averages of at least three different measurements; the standard deviation in all cases was less than 2°). The advancing contact angles of hexadecane were 36° and 43° for SAMs formed from HTS and OTS, respectively, on both PZT and Si/SiO_2 substrates. The receding contact angles for hexadecane were about 20° or less for SAMs formed from both HTS and OTS (not shown in Figure 1). The experiments conducted with SAMs formed from HTS and OTS on Si/SiO_2 substrates were compared with the available published experimental data;[28] the contact angles of water and hexadecane for these substrates were similar to those obtained for SAMs on PZT and also agree with values reported in the literature for SAMs formed on Si/SiO_2 substrates.[28] There is, thus, no difference between the macroscopic wetting properties of the SAMs of the same alkyltrichlorosilane with respect to the substrates on which they are formed (i.e., SiO_2 vs PZT). In both cases, wettability measurements suggested that surfaces with very low free energy are formed.

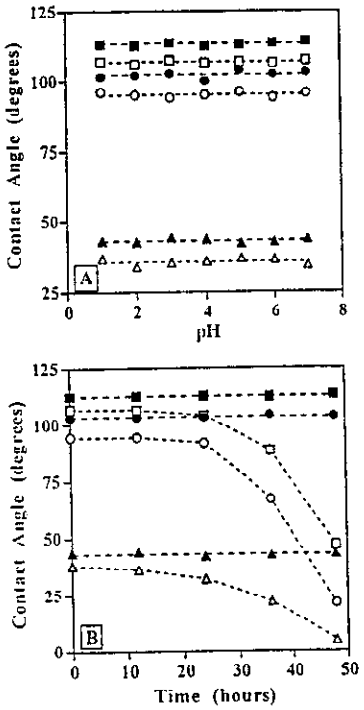

Figure 1. Advancing and receding contact angles of water and hexadecane for SAMs formed on PZT from 1 mM solutions of hexyltrichlorosilane (HTS, open symbols) and octadecyltrichlorosilane (OTS, filled symbols) at 25 °C: (A) SAMs formed from HTS and OTS on PZT were placed in solutions of HCl in which the pH varied from 1 to 7 at room temperature (25 °C) for 2 h. The data shown are the advancing (■, □) and receding (●, ○) contact angles of water and the advancing contact angles of hexadecane (▲, △) measured after exposure to solutions of various pH. (B) SAMs formed on PZT from HTS and OTS were placed in a solution of 0.1N HCl (pH 1, unbuffered), and the change in contact angles of water and hexadecane over time was monitored. Each data point represents an average of at least three measurements (at different locations on the sample). In each case, the standard deviation of the measurements was less than 2°. The dashed lines are drawn only as a guide to the eye.

Figure 1B shows the contact angles of water and hexadecane after long-term exposure of SAMs formed on PZT to solutions of 0.1 N HCl (pH 1). The SAM formed from OTS was stable in HCl even after 48 h, as shown by the constancy of the contact angles of water and hexadecane. On the other hand, exposure to HCl solution (pH 1) of SAMs formed from the short-chain alkylsilane (HTS)

(52) Briggs, D.; Seah, M. P. *Practical Surface Analysis*; John Wiley and Sons: Chichester and New York, 1983.

(53) Wagner, C. D.; Riggs, W. M.; Davis, L. E.; Moulder, J. F.; Muilenberg, G. E. *Handbook of X-ray Photoelectron Spectroscopy*; Perkin-Elmer Corp.: Eden Prairie, MN, 1979.

(54) The ellipsometric thicknesses and contact angles of water and hexadecane for SAMs formed from HTS and OTS on Si/SiO_2 substrates cleaned by the two methods—piranha-cleaned or plasma-cleaned—were similar to each other as well as to published values.[28]

(55) The roughness of the PZT thin film was examined by atomic force microscopy of a plasma-cleaned PZT sample using a Digital Instruments Nanoscope II in contact mode. The average peak-to-valley height was ~200 Å with an average distance between peaks of about 0.5 μm. The roughness and partial transparency of the PZT thin film (thickness 0.4 μm) introduced substantial ambiguities in the estimation of its optical constants (index of refraction and extinction coefficient). Under these conditions, it was not possible to employ ellipsometry to measure the thickness of a SAM of OTS (expected thickness ~26 Å when in extended all-trans configuration). For a detailed discussion of the principles and limitations of ellipsometric measurement of thin films, please see: Azzam, R. M. A.; Bashara, N. M. *Ellipsometry and Polarized Light*; North-Holland: Amsterdam, 1977.

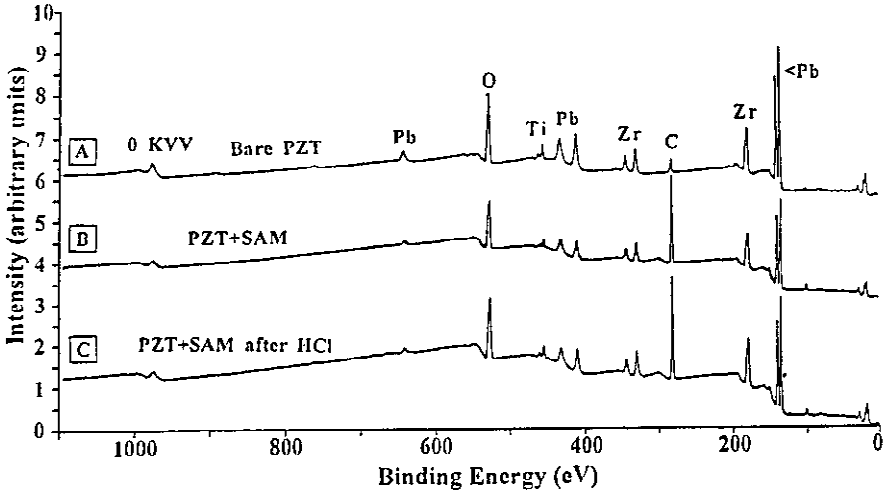

Figure 2. Survey X-ray photoelectron spectra obtained at a takeoff angle of 68° of (A) the bare, air plasma-cleaned PZT sample; (B) the SAM formed on PZT from a 1 mM solution of OTS at 25 °C in a nitrogen atmosphere; and (C) the SAM formed on PZT in the same way as in part B and exposed to a solution of 0.1 N HCl (pH 1) for 12 h. Representative peaks of Pb, Zr, Ti, O, and C are indicated.

rendered them progressively less hydrophobic, presumably because of disruption of the SAM due to etching (see below). After 48 h of exposure to HCl, the advancing and receding contact angles of water were 41° and 22°, respectively, similar to those obtained for an uncleaned surface of the PZT film that has not been treated with the silane. Control experiments performed with Si/SiO_2 substrates did not exhibit this behavior: the SAMs formed from HTS and OTS on Si/SiO_2 were stable after 48 h of exposure to HCl, in agreement with Wasserman *et al.*[28] The cause of the degradation of the SAM formed from HTS on PZT is probably the etching of the underlying PZT by HCl; the short-chain SAM is known to be much more disordered than its long-chain counterpart[27,28] (as suggested by the contact angle data) and may allow penetration by HCl such that it is undermined by progressive etching of the PZT. (This is not seen in the case of Si/SiO_2 substrates because HCl does not etch SiO_2.) The long-chain SAM formed from OTS is more hydrophobic and is likely to be more ordered[27,28] and thus may act as a barrier against etching of PZT by HCl.

We probed the structure and stability of SAMs on PZT by XPS. The survey spectra obtained at a takeoff angle of 68° for bare (control) PZT samples and for SAMs formed from OTS on PZT before and after exposure to HCl (pH 1, 12 h) are presented in Figure 2. The survey spectrum of the bare PZT sample (denoted A in Figure 2) exhibits dominant peaks of Pb, Zr, Ti, and O, along with a C 1s peak due to surface contamination by hydrocarbon species. A very weak Si 2p peak is also detected in spectrum A at ~103 eV binding energy, which we attribute to SiO_2 particulate surface contamination resulting from cleaving and handling of the substrate in atmosphere prior to mounting in the XPS apparatus. The survey spectrum of a SAM formed from OTS on PZT is presented as B in Figure 2. The relative intensity of the C 1s photoelectron peak is considerably higher in spectrum B (compared to A). In addition, angle-resolved spectra (at takeoff angles of 24° and 45°, not shown) reveal that the carbon represented by the C 1s peak is surface-bound. The Si 2p peak also increased slightly in intensity in spectrum B, presumably due to the contribution of terminally bound Si atoms in the OTS. The XPS data are, thus, consistent with the hypothesis that a monolayer of hydrocarbon is formed on the surface of PZT.[28,44,56] The third spectrum (C) in Figure 2 is that of the SAM formed from OTS after exposure to HCl (pH 1) for 12 h. There is no significant difference between the survey spectra B and C shown in Figure 2 and also between the intensity of the C 1s peak in both cases relative to the intensity of the respective Pb 4f peaks. The XPS spectra together with the contact angle data suggest that the SAM formed from OTS on PZT is stable after 12 h in HCl.

The XPS survey spectra of all the PZT samples revealed a surface region slightly rich in Zr. The nominal composition of the sol used to prepare the PZT thin films was $PbZr_{0.4}Ti_{0.6}O_3$. However, the surface layer probed in these experiments was estimated to contain slightly more Zr than Pb (atomic ratio of Zr/Pb = 1.1) and almost no Ti (<5%), using the measured peak intensities at 68° and the sensitivity factors[53] provided for this instrument by the manufacturer. Quantitative analyses relying on such XPS sensitivity factors often have poor absolute accuracy due to variations caused by sample morphology, compositional heterogeneity, and other factors. However, the changes in relative intensity of the various elemental peaks as a function of photoelectron takeoff angle can be used to reliably infer qualitative changes in composition as a function of depth. At higher takeoff angles, the relative content of Pb and Ti increased, while that of Zr decreased. This suggests that while the bulk composition of the film may be close to its nominal composition ($PbZr_{0.4}Ti_{0.6}O_3$), the surface region is depleted in Ti and enriched in Zr. Previous studies of PZT films using XPS and Auger electron spectroscopy (AES) have also indicated a thin surface layer richer in Pb and Zr than the nominal composition might suggest.[57,58]

Angle-resolved high-resolution O 1s spectra at takeoff angles of 24° and 68° for a bare PZT sample are presented in Figure 3. These spectra reveal two different chemical

(56) SAMs formed from OTS on Si/SiO_2 were also probed by XPS. The relative amount of carbon due to surface contamination and that due to the formation of a SAM overlayer were similar for both SiO_2 and PZT samples. Also, the spectra obtained for the SAM on the SiO_2 sample were similar to those in earlier reports.[28]

(57) Qian, Z.; Xiao, D.; Zhu, J.; Li, Z.; Zuo, C. *J. Appl. Phys.* **1993**, *74*, 224–227.

(58) Lau, W. M.; Bello, I.; Sayer, M.; Zou, L. *Appl. Phys. Lett.* **1994**, *64*, 300–302.

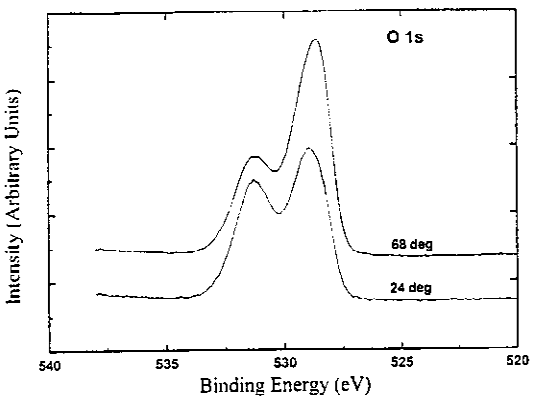

Figure 3. Angle-resolved high-resolution XPS O 1s spectra for a bare, air plasma-cleaned PZT thin film sample at takeoff angles of 24° and 68°. The spectrum obtained at a takeoff angle of 24° has been magnified threefold to enable easy comparison of the two O 1s peaks (Note that no comparison of peak intensities between the two spectra is attempted). There are two oxygen species with BE's of approximately 529 and 531 eV assigned to an oxide and hydroxide, respectively. The increase in intensity of the O 1s peak at 531 eV as the takeoff angle is lowered suggests that the hydroxide species is surface-bound.

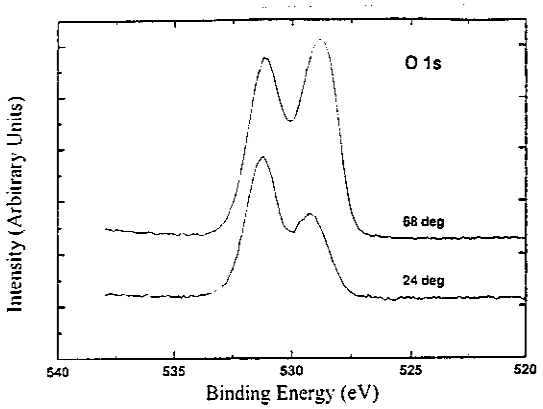

Figure 4. Angle-resolved high-resolution XPS O 1s spectra at takeoff angles of 24° and 68° for a sample of PZT with an overlayer of SAM formed from OTS. The O 1s spectrum obtained at a takeoff angle of 24° has been magnified threefold to enable easy comparison of its two peaks. There are two oxygen species with BE's of approximately 529 and 531 eV, assigned to the oxide and hydroxide, respectively.

states for oxygen in the bare PZT. The photoelectron peak at the lower binding energy (BE ~ 529 eV) can be assigned to an oxide (presumably PZT), and the other (at a BE of 531 eV) to a hydroxide species.[59-63] Zomorrodian and co-workers[64] have assigned an O 1s feature at 531.1 eV in their XPS spectra of laser-ablated PZT films to surface-segregated PbO. However, for our materials the assignment of a hydroxide species near this binding energy is more appropriate. Our angle-resolved XPS data indicate a surface enrichment of Zr, and the Zr 3d spectra discussed below show an additional binding energy state (assigned to *Zr*−OH) whose intensity dependence on angle (surface vs bulk contribution) correlates closely with the intensity variation of the assigned hydroxide feature. In addition, related experiments have shown correlations between the intensity of the ~531 eV O 1s feature and exposure of PZT films to H_2O vapor.[63] The O 1s peak assigned to the hydroxide species increases in intensity relative to the peak assigned to the oxide as the takeoff angle is lowered (68° to 24°), indicating that the hydroxide species are present at the surface of the PZT.[63] Figure 4 presents the high-resolution O 1s spectra for samples of PZT thin films with an overlayer of a SAM formed from OTS at takeoff angles of 24° and 68°. The peak at higher BE due to the hydroxide species shows enhanced intensity relative to the peak at the lower BE at a takeoff angle of 24° as compared to a takeoff angle of 68°. This effect is more pronounced for the PZT sample with the SAM overlayer than for the bare PZT sample (Figure 3). This is due to the presence of the SAM overlayer (~26 Å thick); in this case, the depth to which the PZT is probed by XPS is less than the depth for the case of the bare PZT sample. It is important to note that only the ratio of intensities of the two BE states of the O 1s peak is being compared in Figures 3 and 4; the absolute intensities of the O 1s peaks in Figure 4 are substantially attenuated with respect to those in Figure 3 (compare also the survey spectra shown in Figure 2). The presence of the hydroxide peak (higher BE) in the high-resolution O 1s spectra of PZT samples with a SAM overlayer, thus, suggests that a hydroxide-rich, near-surface PZT layer exists under the SAM (i.e., even after reaction with OTS). The hydroxide peak is likely due to unreacted hydroxide groups on the PZT (see below) and/or uncondensed silanol oxygens introduced by exposure of the surface to OTS. The hydroxide peak is also observed in the high-resolution spectra of the O 1s peak obtained for PZT samples with the SAM overlayer that were exposed to HCl solution (pH 1) for 12 h (spectra not shown).

High-resolution spectra of the dominant peaks of all the metals (namely, the spin−orbit doublets of Pb 4f, Zr 3d, and Ti 2p) were also examined. Both Pb and Ti showed only one chemical state at all takeoff angles used (i.e., only one spin−orbit doublet each, Pb $4f_{7/2}$ = 138.0 eV, Pb $4f_{5/2}$ = 143.0 eV, Ti $2p_{3/2}$ = 458.0, and Ti $2p_{1/2}$ = 463.6 eV), which we assign to their respective oxides in PZT (spectra not shown).[58,65] The angle-resolved high-resolution Zr 3d spectra are presented for bare PZT in Figure 5 (at takeoff angles of 24° and 68°, spectra A and B, respectively) and for PZT with a SAM overlayer in Figure 6 (at takeoff angles of 24° and 68°, spectra A and B, respectively). We found that the spin−orbit split Zr 3d peak exhibits two binding states—one at Zr $3d_{5/2}$ = 180.3 and Zr $3d_{3/2}$ = 182.7 eV and the other at Zr $3d_{5/2}$ = 181.4 and Zr $3d_{3/2}$ = 183.8 eV.

We assign the lower BE doublet of the Zr 3d peak to Zr atoms present in the form of an oxide in PZT. This follows from findings in XPS studies by Murata *et al.* of several perovskite oxides, including $PbTiO_3$.[67] These studies have

(59) Sarma, D. D.; Rao, C. N. R. *J. Electron Spectrosc. Relat. Phenom.* **1980**, *20*, 25−45.
(60) Barr, T. L. *J. Phys. Chem.* **1978**, *82*, 1801−1810.
(61) Au, C. T.; Roberts, M. W. *Chem. Phys. Lett.* **1980**, *74*, 472−474.
(62) Carley, A. F.; Rassias, S.; Roberts, M. W. *Surf. Sci.* **1983**, *135*, 35.
(63) Zavadil, K. R. Unpublished results, 1994. High resolution O 1s spectra were obtained for (i) bare, clean PZT samples, (ii) PZT samples after sputtering for 15 min with 1 keV Ar^+ at ~1 $\mu A/cm^2$, and (iii) the sputtered samples after exposure for 10 min to ~20 Torr of H_2O. Sputtering produces a near-complete loss of the high-BE state of oxygen. Re-exposure to H_2O produces a partially-resolved O 1s state shifted by ~2 eV (i.e. at ~531 eV). The same result was obtained even when sputtering with lower energy (400 eV) ions was performed. Furthermore, angle-resolved spectra of the O 1s peak at takeoff angles of 15, 20, 30, 40, and 90° demonstrate a peak at ~531 eV with progressively smaller relative intensity. It is, thus, clear that the hydroxide species is present in a very thin surface layer.
(64) Zomorrodian, A.; Mesarwi, A.; Wu, N. J.; Ignatiev, A. *Appl. Surf. Sci.* **1994**, *90*, 343−348.
(65) Barr, T. L.; Seal, S.; Chen, L. M.; Kao, C. C. *Thin Solid Films* **1994**, *253*, 277−284.
(66) Chastain, J., Ed. *Handbook of X-Ray Photoelectron Spectroscopy*; Perkin-Elmer Corp.: Eden-Prairie, MN, 1992.
(67) Murata, M.; Wakino, K.; Ikeda, S. *J. Electron Spectrosc. Relat. Phenom.* **1975**, *6*, 459−464.

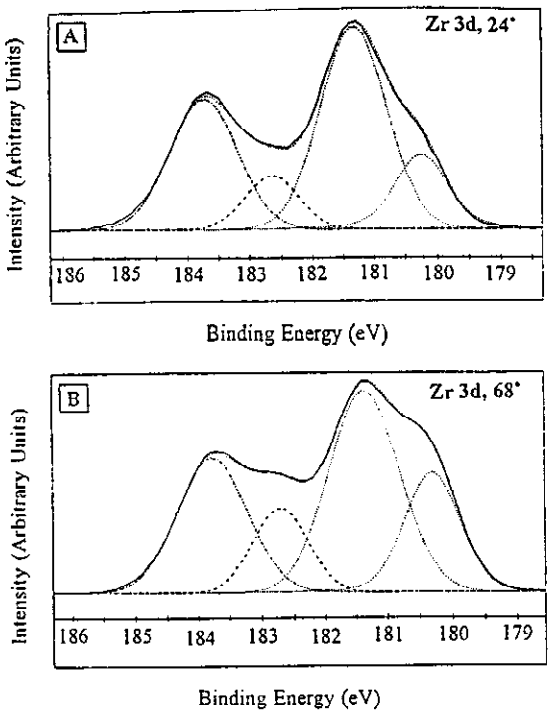

Figure 5. Angle-resolved high-resolution XPS Zr 3d spectra for a bare, air plasma-cleaned thin film of PZT. The two spin–orbit split components of the Zr 3d spectrum (nominal split = 2.4 eV) at each of two takeoff angles (24° and 68°, denoted by spectra A and B) are shown. The peaks were resolved using nonlinear least-squares curve fits for the two binding states of Zr.

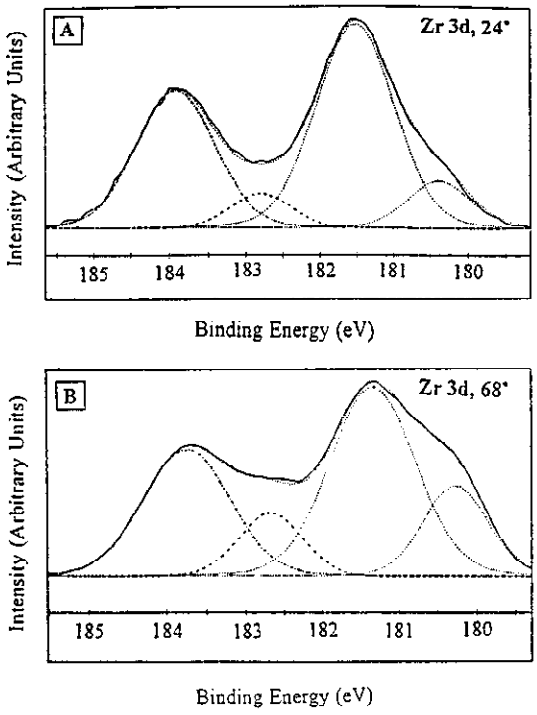

Figure 6. Angle-resolved high-resolution XPS Zr 3d spectra for a sample of PZT thin film with an overlayer of SAM formed from OTS. The two spin–orbit split components of the Zr 3d peak at each of two takeoff angles (24° and 68°, denoted by spectra A and B) are shown. The peaks were resolved using nonlinear least-squares curve fits for the two binding states of Zr.

shown that the BE of the Ti 2p photoelectrons in the perovskite $PbTiO_3$ is shifted toward lower BE by up to about 1 eV relative to that of TiO_2 (rutile). We find a similar downward shift (of ~2 eV) in BE of the Zr 3d doublet in the PZT as compared to the reported BE of the Zr 3d doublet in zirconia (ZrO_2).[66] The second Zr 3d doublet (BE = 181.4 and 183.8 eV) is shifted from the lower BE doublet by about +1 eV. This shift is consistent with a hydroxylated metal species,[62] probably of the form $PbZrO_x(OH)_{3-x}$ (see below). This species is also observed in high-resolution spectra of the Zr 3d peak in PZT samples with a OTS SAM that were exposed to HCl solution (pH 1) for 12 h (spectra not shown).

The angle-resolved spectra of the Zr 3d peak and the fitted curves shown in Figures 5 and 6 indicate that the Zr species at the higher BE (assigned as the hydroxylated Zr species) are present nearer the surface of the PZT thin film relative to the Zr species at the lower BE (the relative intensity of the higher BE peak is greater at a takeoff angle of 24° than at one of 68°). Because this Zr species and the hydroxide species (see O 1s spectra in Figure 3) track each other in relative abundance with respect to the takeoff angle (i.e., at the takeoff angle of 24° the ratio of the intensity of the higher BE peak to that of the lower BE peak of Zr is higher than the same ratio at 68°; and similarly the ratio of the higher BE peak to the lower BE peak of O is greater at 24° than at 68°), it is likely that they exist in the form of a hydroxyl-bearing Zr species at the surface of the PZT. Some of the hydroxyl groups in these species may be exposed at the surface of the PZT thin film. These observations point to the following proposed structure for the surface of the PZT thin film with a SAM overlayer. The OTS molecules react with trace water in the silanation solutions or on the surface of the PZT thin films and, perhaps, with some of the surface-bound hydroxyls to form a monolayer. Underneath the SAM is a very thin layer (a few tens of angstroms) composed of $PbZrO_x(OH)_{3-x}$ and PZT. As the depth of the PZT thin film probed by XPS increases, the hydroxide component decreases, the Ti content increases, and the composition of the PZT film more closely approaches its nominal composition of $PbZr_{0.4}Ti_{0.6}O_3$.

Finally, we employed SEM to monitor the etching of PZT by HCl. Figure 7 presents a series of cross-sectional scanning electron micrographs of the PZT thin film (with and without the SAM overlayer) that has been exposed to a solution of HCl (pH 1) for varying periods of time. Figure 7A shows the PZT thin film (thickness ~4000 Å) with the underlying platinum–titanium electrode (thickness ~4000 Å) on a silicon wafer, prior to exposure to the HCl solution. Figure 7B shows the PZT thin film after exposure to HCl for 24 h; during this interval about 1200 ± 100 Å of PZT can be etched (estimated from three separate experiments). In Figure 7C, it is seen that about 2800 ± 200 Å of PZT has been etched away after 48 h. Figure 7D shows that the PZT thin film with an overlayer of SAM formed from OTS is ~4000 Å thick after exposure to HCl for 48 h. Thus, SAMs formed from OTS are able to act as protective barriers against corrosion by HCl.

Conclusions

Data obtained by wettability measurements and XPS suggest that we have formed uniform SAMs of alkyltrichlorosilanes on the surface of PZT, a complex oxide. The data indicate that the SAMs on PZT are similar to SAMs formed on SiO_2. Angle-resolved high-resolution XPS spectra of the O 1s peak and the dominant peaks of

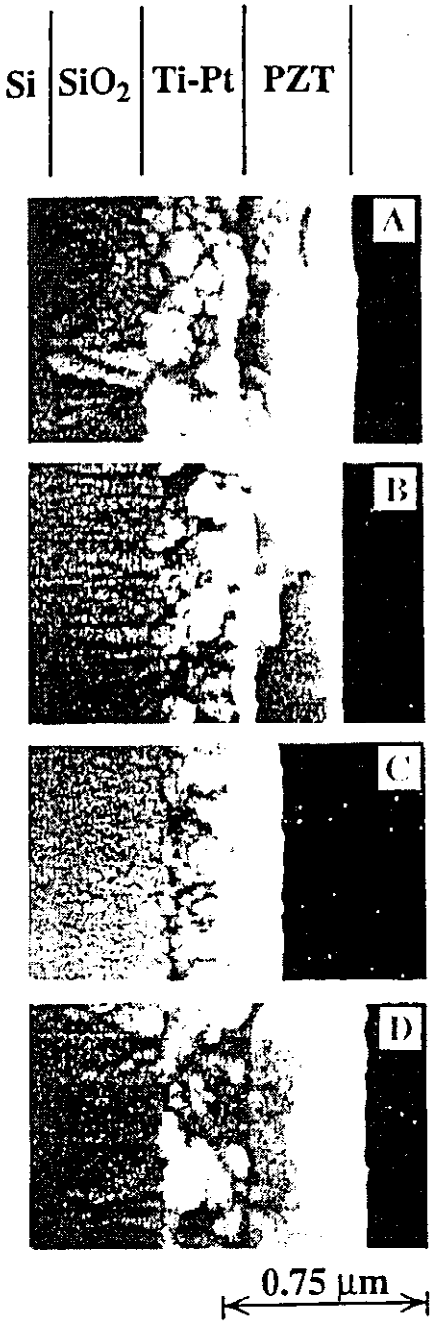

Figure 7. Monitoring of the etching of PZT by 1 N solution of HCl by cross-sectional SEM: (A) SEM micrograph of the PZT thin film (~4000 Å thick) on the $Si/SiO_2/Ti/Pt$ substrate. The Pt–Ti layer is ~4000 Å thick. (B) SEM micrograph of the PZT film after exposure to HCl for 24 h at 25 °C. (C) PZT thin film after exposure to HCl for 48 h at 25 °C. (D) PZT thin film upon which a SAM has been formed from 1 mM OTS solution under nitrogen at 25 °C after exposure to 0.1 N HCl (pH 1) for 48 h at 25 °C. The scale bar shows 0.75 μm.

the metals suggest that the surface of the PZT thin film is deficient in Ti and that, in a thin layer at the surface, Zr is associated with hydroxyls. It is possible that such preferential enrichment of one phase (e.g., $PbZrO_3$) of a multicomponent solid solution (e.g., $PbZr_xTi_{1-x}O_3$) at the surface occurs in other complex oxide materials as well. We believe that it may be possible to form SAMs of alkyltrichlorosilanes on the surface of other complex oxide materials. The data from the analytical techniques used to probe the structure of the monolayers formed on PZT (contact angle, XPS) do not preclude the presence of intercalated hexadecane (the solvent used to dissolve the alkylsilanes used) in the organic monolayers formed. The tendency for noncovalent inclusion of hexadecane into SAMs formed from OTS on silica has been studied by Kallury *et al.*[68] Although our protocol for the formation of the SAMs was designed to promote the removal of physically adsorbed constituents (sonication, extensive washing in carbon tetrachloride and ethanol), we cannot rule out the presence of hexadecane in our monolayers.

We probed the stability of the SAMs in strongly acidic media by wettability measurements, XPS, and SEM. Wettability and XPS data suggest that SAMs formed from the short-chain hexyltrichlorosilane (HTS) are stable for short periods of time (up to 12 h) when placed in a solution of HCl. They then degrade probably due to the etching of the underlying PZT by HCl at defect sites. Wettability measurements appear to be the easiest and most sensitive method of determining the stability of SAMs, in agreement with previous reports.[24-29] The SAMs formed from the long-chain octadecyltrichlorosilane (OTS) are stable in HCl for long periods of time (over 3 days). By use of SEM, we have demonstrated that SAMs formed from OTS are able to protect PZT from etching by HCl.

Ferroelectric oxide materials such as PZT have been proposed for numerous device applications. In these endeavors, it is necessary for the thin films of these oxides to be stable in various chemical environments. It is also important that modification of the surface of the thin films be amenable to micropatterning. Furthermore, the modified surfaces may be called upon to participate in further processing steps, e.g., as templates for the deposition of layers of other metal or oxide conductors or photoconductors. Studies are currently underway to establish whether SAMs of organosilanes are useful in such efforts. Organosilane SAMs provide flexibility with respect to control of surface properties through use of different terminal functional groups of the alkylsilane, by formation of mixed monolayers, and by micropatterning SAMs of alkylsilanes with different terminal functionality on the same surface.

Acknowledgment. This research was supported by the Sandia/University Research Program and the University of New Mexico and by the National Science Foundation (Grant HRD-9450475). The Sandia National Laboratories are operated for the U.S. Department of Energy under Contract Number DE-AC04-94AL85000. We gratefully acknowledge Paolina Atanassova and Kevin Zavadil for fruitful discussions of the XPS data.

LA951072K

(68) Kallury, K. M. R.; Thompson, M.; Tripp, C. P.; Hair, M. L. *Langmuir* **1992**, *8*, 947–954.

APPENDIX B

Template-Assisted Electrochemical Deposition of Ultrathin Films of Cadmium Sulfide

Joseph Cesarano III,[†*] Xiang Xu,[‡] Eileen Burch,[†] and Gabriel P. Lopez[‡*]
[†]Dept. 1831, Sandia National Laboratories, Albuquerque, NM and
[‡]Dept. of Chemical & Nuclear Engineering, University of New Mexico, Albuquerque, NM

Abstract

Uniform thin films of cadmium sulfide were prepared by template-assisted electrochemical deposition on gold electrodes covered with Langmuir-Blodgett (LB) films. An electrolytic cell was used for the production of low concentrations of S^- to effect heterogeneous crystallization on LB films, while preventing homogeneous precipitation. 3,4 and 5 layer LB films of cadmium arachidate were investigated. Charcterization of deposited films by optical microscopy, atomic force microscopy and energy dispersive X-ray analysis of film composition indicated that a variety of different types of CdS films can be produced depending on the type of LB film used, the electrode at which template-assisted deposition is carried out, the magnitude and frequency of alternating potentials used, and the deposition time used. In general, hydrophilic organic films that present cadmium carboxylate groups to the deposition surface (i.e., 3 and 5 layer LB films) supported crystallization of CdS, while those that present hydrophobic, methyl groups (i.e., 4 layer LB films and self-assembled monolayers of alkanethiolates on gold) did not. The best methods for the rapid deposition of conformal, ultrathin films (< 100 nm) of CdS used highly-ordered 5 layer LB films at grounded electrodes. The data presented suggest that templating with LB films, when used together with electrochemical deposition, has potential for the convenient production of oriented crystalline thin films of cadmium sulfide and similar materials.

1. Introduction

Thin, conformal, crystalline films of cadmium sulfide (CdS), a II-IV semiconductor compound, are of interest as functional components in a variety of opto-electronic devices such as solid state lasers and detectors,[1] solar cells,[2,3,4] and optical memories.[2] Methods for generating these films have included chemical vapor deposition,[5] plasma sputtering,[6] electrodeposition,[7] and precipitation.[2,3,4] Techniques for preparing films based on heterogeneous crystallization from liquid solutions have several potential

advantages over vapor phase deposition techniques including the ability to form crystalline films at low temperature over large area substrates. The ability of organic functional groups to facilitate and mediate heterogeneous nucleation from aqueous solutions at solid substrate [8,9] also has the potential to enhance uniform nucleation (crystallite type, orientation and distribution) of CdS and thus lead to superior performance of thin films in device applications. For example, Langmuir-Blodgett (LB) films have been investigated extensively for the controlled nucleation of CdS and have been demonstrated to be useful for the formation of nanoparticles of CdS. One particularly effective methodology for the formation of planar arrays of Q-state particles of CdS has been the exposure of LB films comprised of cadmium arachidate layers to gaseous H_2S.[10,11,12]

We have examined several methods for template-directed heterogeneous crystallization of CdS and present here a report of preliminary work on a new technique that has produced uniform thin films of CdS through relatively short deposition times. The technique is an extension of that described by Fatas *et al.* [7] for the *in situ* generation of low concentrations of Cd^{2+} and S^{2-} by alternating current electrolysis and the subsequent formation of thin CdS films from these precursors. We have examined the effectiveness of several schemes for improving the quality of thin films produced by this technique by the use of template-directed nucleation at the surface of various types of LB films. LB films were prepared by several methods by dipping of gold-coated silicon wafers that had been rendered hydrophobic by the formation of self-assembled monolayers (SAMs) by reaction of the gold surface with $HS(CH_2)_{15}CH_3$.[13,14] The primary characterization techniques we have employed thus far in our studies (atomic force microscopy, optical microscopy and energy dispersive X-ray analysis of film composition) suggest that when combined with *in situ* electrochemical generation of ionic precursors for CdS, organic template-assisted heterogeneous precipitation of CdS at electrode surfaces is a simple, quick method of generating thin films of CdS in which deposition is restricted primarily to areas of the electrode surface modified with organic template moieties.

2. Experimental

2.1. Materials

Chemicals used were arachidic acid (Aldrich Chemical Co., Milwaukee WI), hexadecyl mercaptan (Sigma, St. Louis MO), cadmium chloride (Aldrich), sodium bicarbonate (Fisher, Pittsburgh PA), sodium chloride (J.T. Baker, Phillipsburg NJ), sodium thiosulfate 5-hydrate (J.T. Baker), ammonium sulfate (J.T. Baker), and cadmium sulfate (J.T. Baker). All chemicals were used as received. Silicon wafers (100) (MEMC Electronic Materials Inc., Malaysia) were used as substrates for the gold films. Gold films (600 to 1000 Å) were deposited by thermal evaporation of gold (99.999%, Academy Precision Materials, Albuquerque NM) under vacuum onto silicon wafers that had previously been

coated with an adhesion promoter (50 Å of chromium). Samples for use in LB film deposition were treated with dilute ethanolic solutions (1 mM) of hexadecyl mercaptan to form a hydrophobic self-assembled monolayer. A platinum film (~1000 Å) on a silicon wafer was used as a counter electrode in electrochemical generation of CdS precursors.

2.2. Langmuir-Blodgett Films

The Langmuir-Blodgett films of cadmium arachidate were deposited from a Nima 2011 Langmuir trough. For the 3-layer and 4-layer LB films, the subphase was prepared by adding cadmium chloride to deionized water (18.2 MΩ/cm) such that the final concentration of cadmium was 1×10^{-4} M. The pH of the subphase thus prepared was 5.5 and was not further adjusted. To obtain more uniform templating surfaces (see Results and Discussion), 5-layer LB films were also investigated. For 5 layer LB films, the subphase cadmium concentration was 2.5×10^{-4} M and the pH of the subphase was adjusted to 6.5-7.0 by addition of 0.1M $NaHCO_3$ solution. For all depositions, the barrier speed was set to 50 cm^2/min for compression and the deposition pressure was 30mN/m. The upward and downward dipping speeds of the hydrophobic substrate were 1.6mm/min.

LB films comprised of 3, 4 and 5 layers of Cd-arachidate were investigated. The 4-layer LB film had a hydrophobic outer surface and was transferred from the LB trough to the deposition solution directly. The 3 and 5 layer LB films had hydrophilic surfaces and thus were not stable when exposed to air.[13] We therefore transferred the substrate under water (in a small beaker) from the LB trough to the deposition solution.

2.3. Deposition of Cadmium Sulfide

CdS deposition solutions were made according to the method of Fatas, *et al.* Solutions A and B were mixed in a 1:3 ratio by volume.[7] Solution A consisted of 0.01 M $CdSO_4$ and 0.17 M $(NH_4)_2SO_4$ in deionized water and solution B consisted of 0.35 M $Na_2S_2O_3$ and 0.75M NaCl in deionized water. Each solution was stirred for approximately 5-10 minutes until the solids were completely dissolved. CdS deposition solutions were prepared by combining the two solutions A and B and stirring for at least 10 minutes. When solution B was mixed with solution A, the $S_2O_3^{2-}$ ions produced S by the disproportionation reaction:[7]

$$S_2O_3^{2-} \Leftrightarrow S + SO_3^{2-}$$

During the film deposition under reducing potentials, S was reduced to S^{2-} by the following reaction:

$$S + 2e^- \rightarrow S^{2-}$$

A potentiostat (EG&G, Princeton Applied Research Model 173) was used to produce alternating positive and negative square wave potentials on either the electrode coated with the LB film or on the uncoated electrode relative to a ground electrode. The reference electrode was combined with the counter electrode from the potentiostat to form the "charged" electrode which was subjected to the voltage cycles relative to the working ("ground") electrode. For all depositions, the same solution concentrations were used (as described above) and the duration in the voltage cycle of the positive voltage was 2 s, while that of the negative voltage was 1 s. Several potentials (positive and negative) and deposition times were examined. The optimized deposition conditions are reported herein.

For the depositions onto 3- and 4-layer LB films, the ground electrode was a bare platinum film, while the charged electrode was the gold film covered with the SAM and the LB film. In these depositions reduction of S to S^{2-} thus occurred at the gold electrode (presumably at defect sites in the SAM covering the electrode). For the deposition onto the 5 layer LB film, the electrodes were reversed and the bare Pt film was used as the charged electrode and the gold film coated with the LB film was the ground electrode. In this case, the reduction of sulfur occurred at the bare platinum electrode and thus may have resulted in an increased concentration of S^{2-} relative to the depositions on 3 and 4 layer LB films.

2.4. Analysis of CdS Films

The CdS films were examined with an atomic force microscope from Digital Instruments Inc. (model: Nanoscope II). Direct contact imaging was done both in height mode and in force mode, and both types of images are presented herein. In general, height mode images reveal information on the vertical topography of the surface of the films and was used herein to estimate the thickness of conformal films, while force mode provides sharper images of features on the surface of the films and was used in high resolution imaging.[15] For imaging at low magnifications, the scanning speed was 2.48 Hz. No data filtering was used during scanning. The integral, proportional, and 2D gains were tuned to the highest possible values for the height mode, but the lowest possible values for the force mode.[15]

At high magnification, the AFM was used to image the crystalline lattice of the deposited CdS. For these experiments, the AFM was calibrated versus a standard mica sheet. To minimize thermal and mechanical drifts of the microscope, the scanning was performed for at least two hours before taking the image and scanning was conducted at a high speed (39.06 Hz) and on a relatively large area (32x32 nm^2). The force mode was used and during data collection the input, high pass, and low pass filters were off. To obtain the high resolution image of the crystalline lattice of CdS (Figure 4B), the raw data (Figure 4A) was subjected to a 2D Fourier transform and principal wave numbers thus obtained were selected and used to perform an inverse 2D Fourier transform to result in the filtered image of the crystalline lattice.

The CdS films were also examined by optical video microscopy using a Nikon Optiphot 66 and image analysis system. Films were characterized using energy dispersive X-ray analysis (EDAX) using an AMRAY 1500 scanning electron microscope.

3. Results and Discussion

We examined a variety of deposition conditions and configurations and present below a synopsis of the results from four different types of deposition experiments that demonstrate the utility of organic templates in influencing CdS film formation during electrodeposition. Table 1 lists the experimental codes and conditions for the four different types of depositions we will discuss below. Deposition conditions varied in the nature of the deposition surface examined, in deposition time, and in the magnitude of the alternating voltage used. For each deposition surface (e.g., organic template vs. noninteracting functional group), the deposition conditions for the experiments presented were those found by trial and error optimization to give rise to rapid deposition (when deposition occurred at all) of CdS films. Figure 1 shows schematic diagrams of the electrodeposition cells used in the various deposition experiments.

Table 1: Summary of the experimental conditions for the four types of electrochemical depositions.

Experimental Codes	BARE-Au	3-LB	4-LB	5-LB
Deposition Surface	Plain Au	Cd-carboxylate (3 layer LB film)	Methyl (4 layer LB film)	Cd-carboxylate (5 layer LB film)
Deposition Time	1 minute	1 minute	5 minutes	5 minutes
Voltage Cycles	1V,2s / -1V,1s	1V,2s / -1V,1s	1.75V,2s / -1.75V,1s	2V,2s / -2V,1s
Electrode used for CdS Deposition	Charged	Charged	Charged	Ground
Reducing Electrode for S	Plain Au	Au with SAM	Au with SAM	Plain Pt
Results	Loose particles	Layered single crystallites with crystalline surfaces	No deposition on LB film	Homogeneous conformal thin film

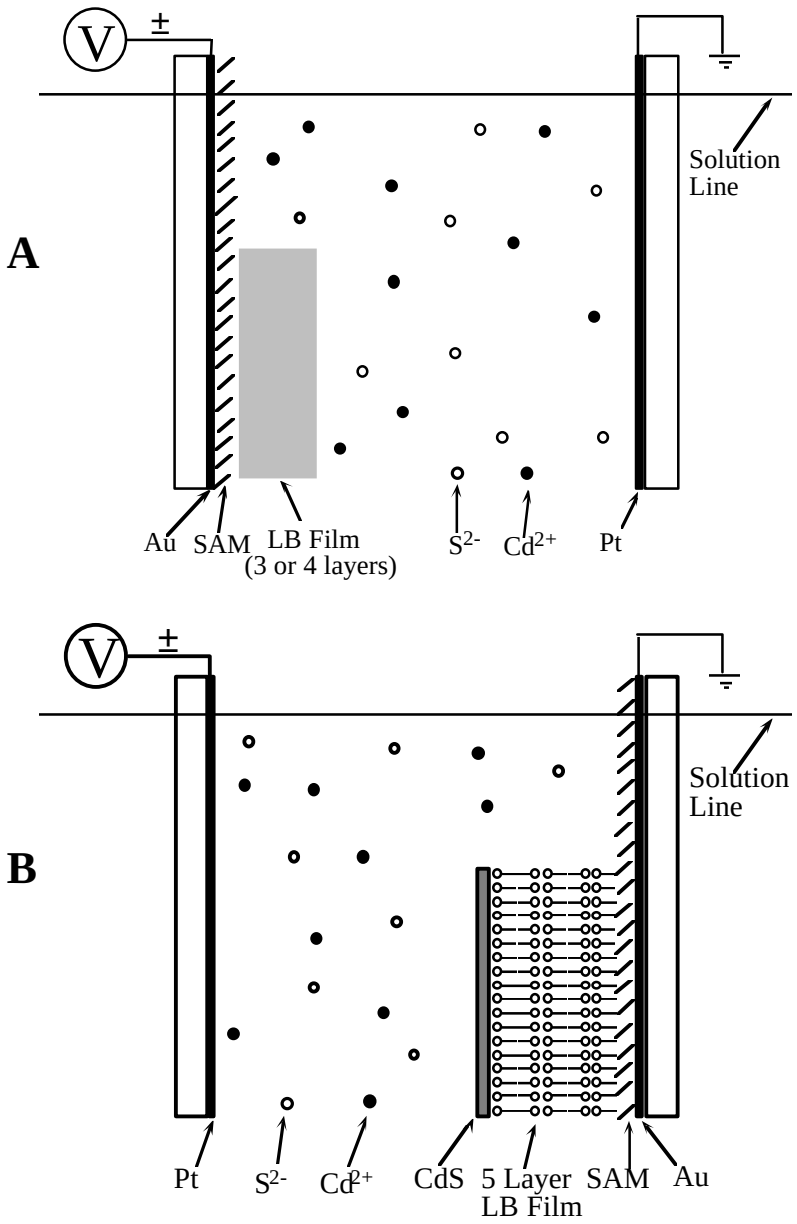

Figure 1: Schematic diagram of the electrochemical deposition cells investigated. In all depositions, the left electrode (referred to as the charged electrode) was subjected to an alternating (square wave) potential cycle relative to the ground electrode (right) to effect the deposition (see Table 1 for voltage magnitudes and durations and the total deposition times). **A.** Deposition cell used for the BARE-AU, 3-LB, and 4-LB experiments. For the BARE-AU experiment, no SAM or LB film was present on the left electrode. For the 3 - LB experiments, a 3 layer LB film, terminated with cadmium carboxylate groups, was deposited on a portion of the left gold electrode, whose entire surface had been subjected to modification by formation of a SAM of hexadecane thiolate. For the 4-LB experiments, a 4 layer LB film, terminated with methyl groups, was deposited on the SAM-modified gold electrode. **B.** Deposition cell used for the 5-LB experiments. For these experiments, the gold film was used as the right (ground) electrode. The ground electrode was modified first by formation of a SAM, and then by formation of a 5 layer LB film, terminated in cadmium carboxylate groups, on a portion of the electrode surface. Note that in all cases, other ionic species (see Experimental section) were also present in the deposition solution.

3.1. Electrodeposition of CdS

Initial experiments focused on examining CdS films formed in a deposition cell similar to that used by Fatas *et al.*[7] We used alternating voltage cycles, and deposition times that had previously been shown by cyclic voltammetry to be sufficient for the electrolytic formation of low concentrations of S^{2-}.[7] The basic setup for these depositions (referred to as BARE-AU), which were performed on a bare gold electrode (i.e., not modified with a SAM or an LB film) is indicated in Table 1 and in Figure 1A.

Figure 2 shows an optical micrograph of the material deposited in the BARE-AU experiment. After 1 min, sparse amounts of material were observed to deposit on the bare gold electrode. Deposition was restricted primarily to the surface of the charged electrode, suggesting a deposition mechanism influenced by the electrochemical nature of the deposition cell. Deposited material exhibited uneven coverage of the gold surface, and when removed from solution and dryed, exhibited poor adhesion to the electrode surface. (Particles were removable from the surface by light blowing.) In the remainder of experiments, we attempted to identify deposition conditions that took advantage of the biomimetic, template-assisting qualities of carboxylate-terminated LB films for producing deposited films with superior qualities (conformal coverage, crystallinity, adhesion).[8,9]

3.2. Template-Assisted Electrochemical Deposition of Crystalline CdS

The first template-assisted depositions investigated (referred to as 3-LB) were ones in which the gold film used as the charged electrode was modified first by the reaction of the gold with $HS(CH_2)_{15}CH_3$ to form a hydrophobic SAM, and then by forming a three-layer LB film of cadmium arachidate on a portion of the electrode. This procedure resulted in a surface of exposed cadmium carboxylate groups for use as templates for nucleation of CdS (see Figure 1A). Electrochemical deposition at this modified electrode was then performed under conditions (voltage cycles, duration) similar to those used in the BARE-AU deposition.

Figures 3A and 3B show optical and atomic force micrographs, respectively, of CdS deposited under the 3-LB conditions at the boundary region of the electrode between areas that were, and were not, modified with the three-layer LB film. These micrographs show that deposited material was restricted primarily to the surface of the LB film and that this material consisted of roughly evenly spaced clusters that were ~ 1 μm in lateral dimension. Analysis of this sample by energy dispersive X-ray analysis (EDAX) suggested that the material formed on the LB film was composed of cadmium and sulfur. Elements (Na, Cl, O, N) of other ions present in the deposition solution were not detected. No cadmium or sulfur was detected on the surface of the SAM. The CdS formed on the surface of the LB film exhibited better adhesion than that produced from the BARE-AU deposition, and in general the deposition rate was higher for the template assisted deposition than for the BARE-AU deposition. These results suggest a template-mediated deposition mechanism on the surface of the LB film.

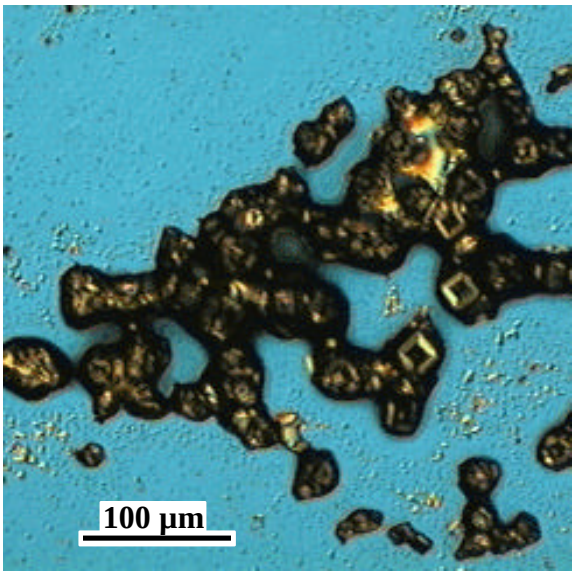

Figure 2. An optical micrograph of material deposited by electrochemical deposition. No organic template was present on the deposition surface. See Table 1 for experimental conditions (BARE-AU).

Figure 3C is an atomic force micrograph of a typical single particle of CdS formed by the 3-LB depositions. The micrograph shows that the particles formed were layered in structure and suggest that the particles were crystalline. This was later confirmed by high resolution AFM (see Figure 4 below). AFM imaging in height mode (micrograph not shown) suggested an average crystallite thickness of ~30 nm for this sample and that the average single layer thickness was 7Å. It is interesting to note that the average crystallite thickness (30 nm) and the layer thickness (7Å) suggest that ~40 layers were deposited in each crystallite of CdS. This number of layers is approximately equal to twice the number of voltage cycles performed during the 1 min deposition. This result may suggest an influence of the electric field created during the voltage cycling on the deposition mechanism. We have no additional data to support this possibility at this time, however, but we plan to continue investigation of the deposition mechanism.

At this point it is important to note that, although deposition under the 3-LB experimental conditions was repeated carefully several times, the resultant films were highly variable (i.e., exhibited wide differences in deposition amount). When substantial material was indeed deposited, the micrographs shown in Figure 3 (and in Figures 4 and 5 below) are typical of the crystalline structures obtained. The high degree of variability in the results obtained for the 3-LB depositions may have been due to one or more of several factors, including variability in the number or type of defects present either in the SAM (the presumed loci for electrochemical reduction of S to S^{-2}) or in the LB film. In subsequent experiments, (e.g., for the 5-LB depositions), we took measures to avoid the presence of such defects in the LB film (see below).

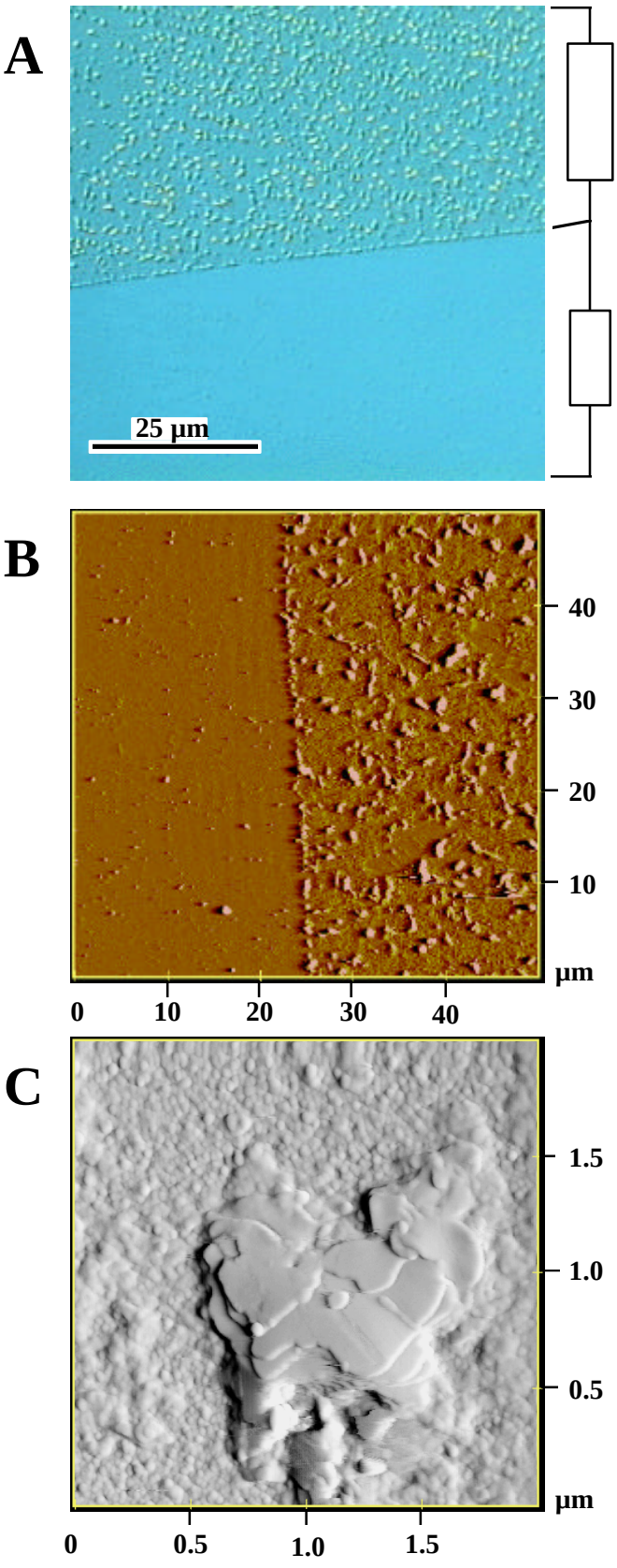

Figure 3. Optical and atomic force micrographs of CdS deposited by template-assisted electrochemical deposition onto a 3 layer LB film. The carboxylate groups terminating the LB film (i.e., exposed at the LB film-water interface) act as templates that mediate the CdS nucleation. See Table 1 for deposition conditions (3-LB). **A.** Optical micrograph of a region showing CdS deposited on LB film-modified areas of the sample and SAM-modified areas of the sample. CdS deposition was generally restricted to the surface of the LB film. **B.** An atomic force micrograph (force mode imaging) of a region similar to that showed in Fig. 3A. **C.** An atomic force micrograph (force mode imaging, higher magnification than 3B) of an individual, layered crystallite of CdS formed on the 3 layer LB film. The background roughness observed is probably at least partially due to the structure of the surface of the gold electrode.

Figure 4 shows a high resolution atomic force micrograph of the crystalline lattice on the surface of a typical crystallite formed in the 3-LB depositions. Fig. 4A presents the raw data (force mode) obtained through the high resolution imaging and Fig. 4B presents the image of the crystalline surface after the raw data was subjected to a Fourier transform filtering protocol.[15] When taken together with the results of the elemental analysis performed, the images obtained by high resolution AFM suggest that the deposited material is indeed crystalline CdS and that the crystals are oriented with a centered rectangular crystalline face parallel to the surface of the LB film. The centered rectangular lattice observed (4.67 X 7.16Å) is similar to that previously published for the (110) crystalline face of the greenockite polymorph of CdS (4.14 x 7.17Å).[16] This data suggests that the template-assisted deposition conditions may be capable of producing uniformly crystalline thin films of CdS, and that the crystalline phase obtained by template-assisted electrochemical deposition may be slightly different from naturally-occuring phases.

Although the crystallite imaged in Figure 3B was typical of those observed for the 3-LB depositions, other layered and non-layered structures were also observed. Figures 5A and 5B show atomic force micrographs of another type of layered crystallite produced in the 3-LB depositions. In these crystalline structures, the primary layered structure appears not to be parallel to the electrode surface. Comparison of Figure 5A, acquired from the structure initially, to Figure 5B, taken after repeated scanning of the sample, shows the ability of the AFM tip to remove successive layers of the stratified material.

While it may be that the material imaged in Figs. 5A and 5B, has the same crystallographic structure as the CdS imaged in Figures 3 and 4, the material imaged in Fig. 5C appears to be a different form of CdS, or perhaps another material entirely. The material shown in Fig. 5C constituted the most conspicuous minor component of the material deposited in the 3-LB depositions. Features with this sort of morphology, which were typically much larger than the major component shown in previous figures (compare scales in 5C with 5A and 5B), constituted less than one percent of the deposited structures. These structures showed no clear layered morphology, and we were unable to obtain a crystalline lattice upon imaging at high resolution with AFM. The fact that the vast majority of deposited crystallites were of similar size and morphology and that these other minor constituents of larger size were present at much lower concentration suggests that template-assisted deposition may be used to deposit crystalline materials with very narrow particle size distributions.

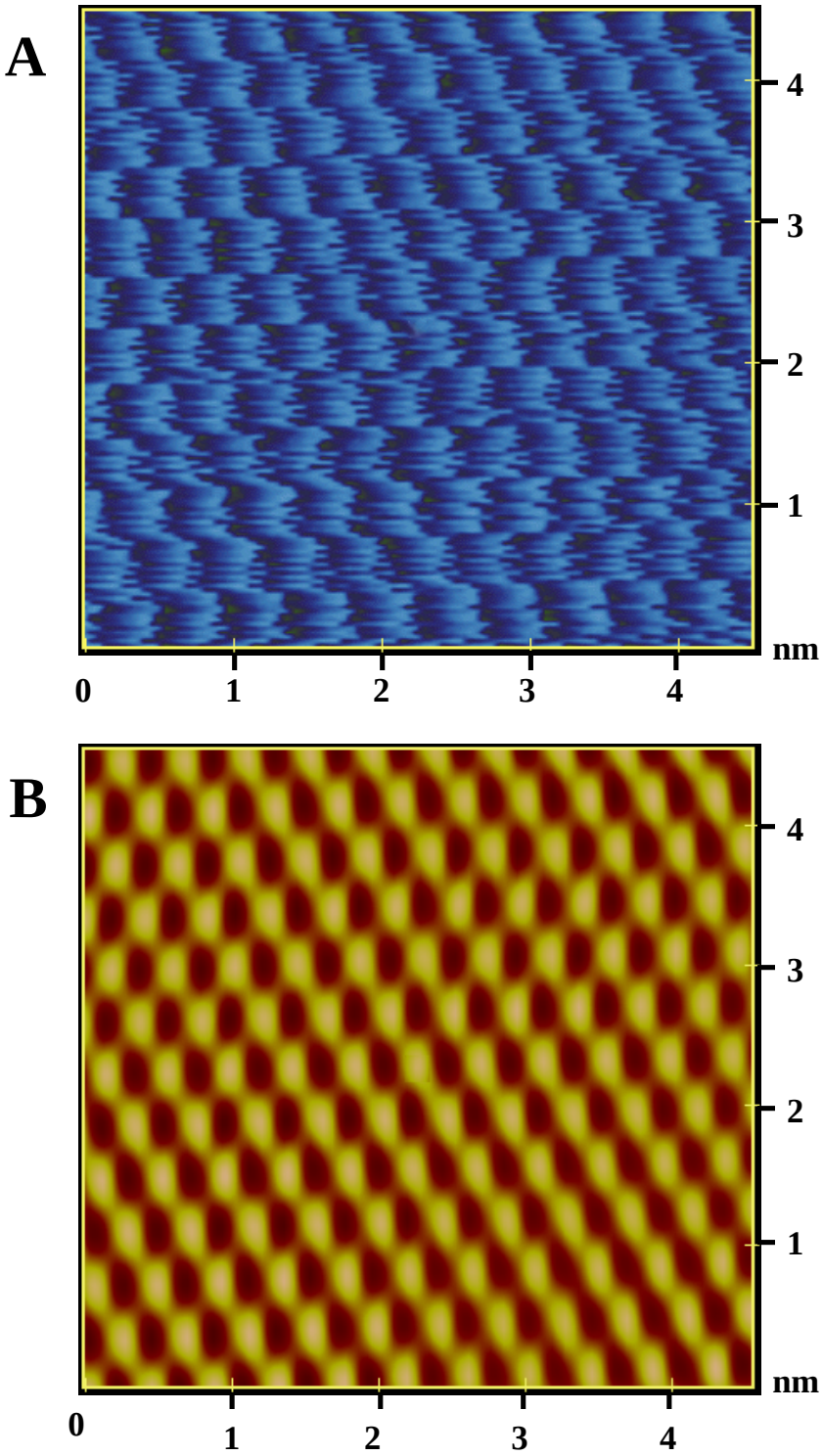

Figure 4. High resolution atomic force micrograph showing the crystalline lattice of CdS deposited on a 3 layer LB film. See Table 1 for deposition conditions (3-LB).**A.** Unfiltered image of the CdS lattice obtained by high resolution imaging of a crystallite such as the one shown in Fig. 3C. **B.** The image of the CdS crystalline lattice (same area shown in 4A) after filtering by a 2D Fourier transform filtering routine.

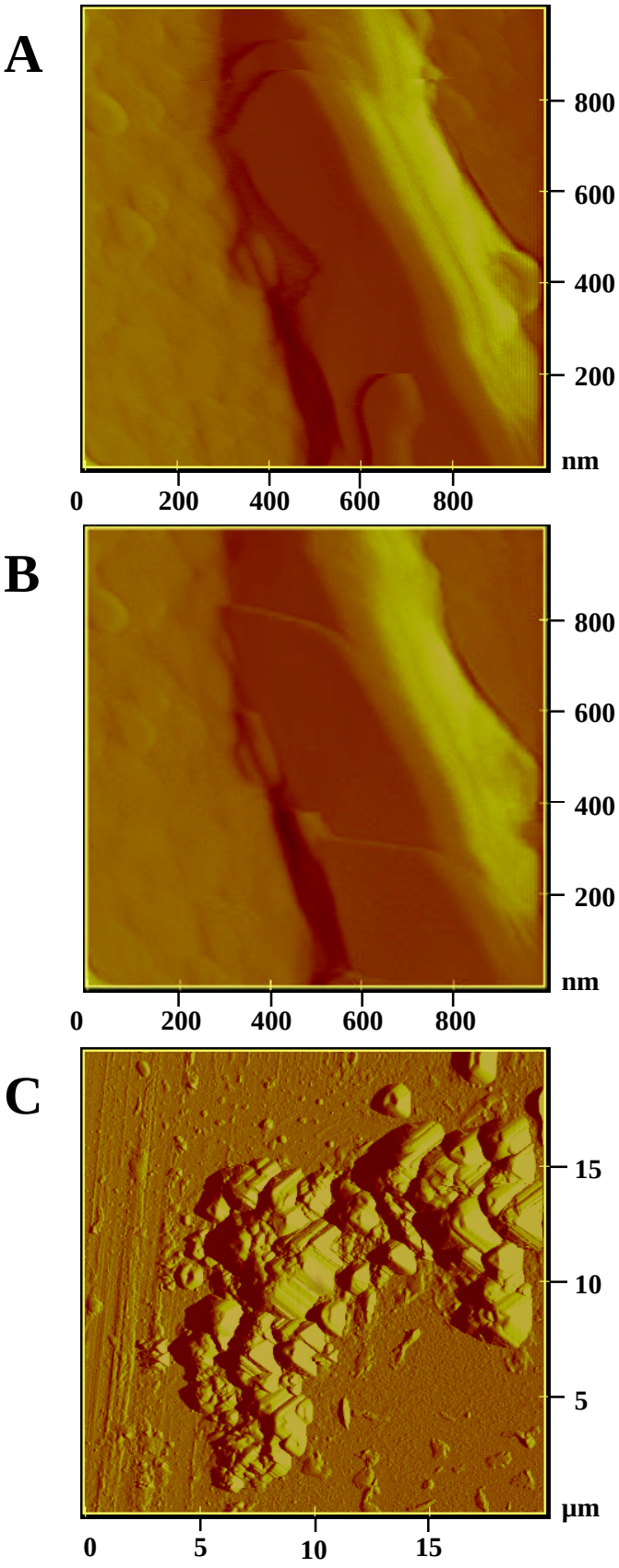

Figure 5. Atomic force micrographs of other features observed of material deposited on the 3 layer LB film. **A.** A crystalline feature similar in size to that in Fig. 3C. **B.** Change in the structure of the feature shown in 5A after prolonged scanning under AFM. This micrograph shows that the AFM can affect the structure of the crystallites. In this case, AFM resulted in the removal of layers of the crystalline material (compare Figs. 5A and 5B). **C.** Structure of a minor constituent produced in the 3-LB depositions. In contrast to the structure of crystallites observed as the major constituent of the deposited material (see for example Fig. 3C and Figs. 5A and 5B), these structures (typically much larger than the crystallites constituting the major component) were observed only infrequently; less than one percent of the deposited features exhibited this structure.

In order to further examine the hypothesis that the carboxylate groups on the surface of the 3-LB samples were indeed participating in template-assisted deposition, we performed an experiment (4-LB) which used deposition conditions similar to those used for the 3-LB experiments, with the exception that the charged electrode was covered with a four layer LB film. The outer surface (interfacing with the deposition solution) of this LB film is terminated in hydrophobic methyl groups. Under the conditions (voltage cycle, deposition time) used for the 3-LB depositions, no easily detectable amounts of material were formed, either on the LB film or on the SAM. Only after the amplitude of the voltage cycle ($\pm$ 1.75 V) and the deposition time (5 min) were increased, did detectable amounts of material become deposited. Figure 6 shows an optical micrograph of the boundary region between the LB film and the SAM underlayer of such a sample after it had been subjected to the 4-LB conditions. It is clear that under similar deposition conditions to those used in the 3-LB experiment, an LB film terminated with hydrophobic methyl groups (4-LB) inhibited the crystallization of CdS. On the areas of the electrode covered with only the SAM, only sparse amounts of material were deposited, presumably at defect sites. These results when taken together with those presented above, strongly suggest a nucleation or deposition mechanism that is mediated by the carboxylate or carboxylic groups on the surface of the 3 layer LB films.

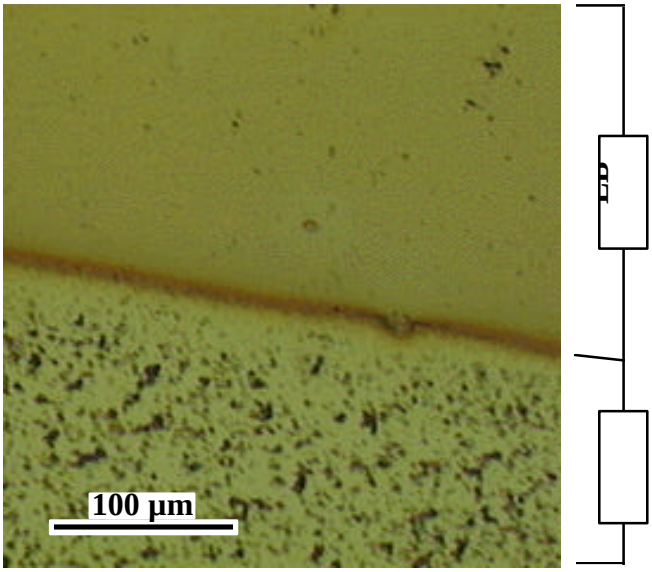

Figure 6. An optical micrograph of a portion of a 4 layer LB film (terminated in methyl groups) and a portion of a SAM after they had been subjected to conditions that produced deposition of crystalline CdS particles on 3 layer LB films. See Table 1 for deposition conditions (4-LB).

3.3. Conformal CdS Thin Films Produced By Template-Assisted Electrochemical Deposition.

The final deposition conditions investigated used information gained in previous experiments to obtain uniform thin films of CdS by template-assisted electrochemical deposition. 5-layer LB films terminated in cadmium carboxylate groups were fabricated and used as templating surfaces. 5-layer LB films are thought to be, in general, more ordered on a molecular level than three layer films,[17] and our aim was to obtain as uniform a templating surface as possible in order to enhance uniform nucleation and crystallization of CdS.[18] The dipping conditions for forming the LB films (concentration of Cd^{2+}, pH) were also adjusted to values known to produce more ordered LB films (see Experimental section). Furthermore the LB films (formed on a SAM-modified Au film) were deposited onto gold electrodes that were now used as the ground electrodes in the deposition cell. A bare platinum electrode was used as the charged electrode so that reduction of S to S^{2-} proceeded unhindered by a dielectric SAM or LB layer. Figure 1B gives the schematic of the deposition setup for the 5-LB depositions (see also Table 1).

Figure 7 shows that, by making these changes, we were able to fabricate conformal thin films of CdS by template-assisted electrochemical deposition at relatively high deposition rates on the LB films. Furthermore, these deposition conditions (summarized in Table 1) produced a high level of reproducibility in making these thin films. Figures 7A and 7B show optical and atomic force micrographs, respectively, of the boundary region between the LB film-covered area of the electrode and the area of the electrode that was modified with only a SAM. These micrographs indicate that the amount of material deposited was much greater on the 5 layer LB film than on the hydrophobic SAM and, that uniform conformal thin films were deposited on the 5 layer LB films. EDAX suggested that the material that was deposited on the LB film was CdS, in that Cd and S were detected while no other elements (Na, Cl, O, N) from ions in the deposition solution were detected. AFM measurements (height mode, data not shown) of this boundary region indicated that the average thickness of the deposited film was ~40 nm.

Although the fact that the deposited material (presumably CdS) was restricted primarily to the LB film area suggested a template-mediated deposition mechanism, the morphology (particle shape and surface features, see Figure 7C) of the material was different from that of the crystalline CdS deposited in the 3-LB depositions. Furthermore, we were not able to obtain an image of the crystal structure of the surface with AFM as we did for the 3-LB sample. We are currently investigating further the possible structure and the deposition mechanism of the CdS thin films obtained under the 5-LB deposition conditions. One possibility is that the higher S^{2-} concentration produced in the 5-LB depositions favored homogeneous nucleation of CdS and the deposited film is composed, at least in part, of crystallites nucleated in solution. These crystallites, perhaps deposited by a physical adsorption mechanism, would be less likely to have uniform crystallographic orientations than crystallites that nucleated on the underlying, ordered LB film.

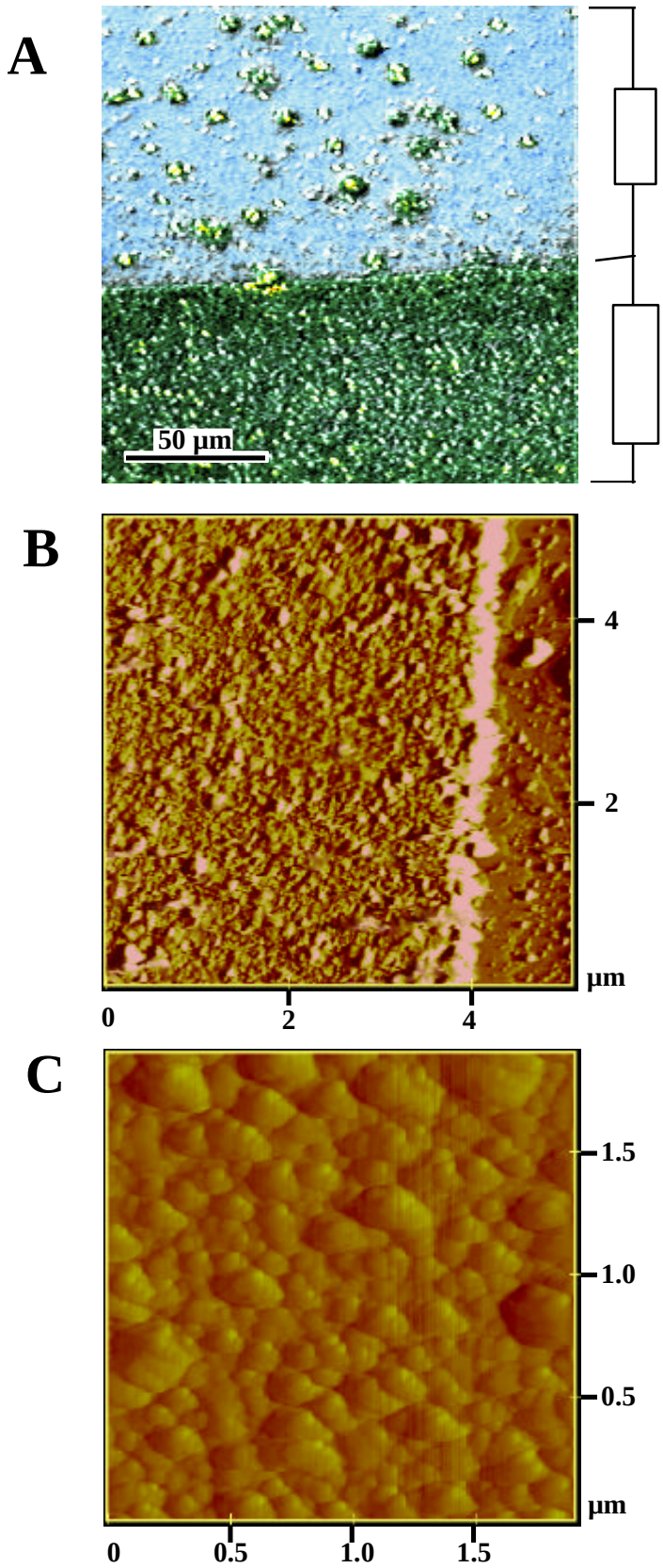

Figure 7. Optical and atomic force micrographs of a uniform thin film (~40 nm in thickness) of CdS deposited by template-assisted electrochemical deposition onto a 5 layer LB film. See Table 1 for deposition conditions (5-LB). **A.** Optical micrograph of a region showing CdS deposition on LB-modified areas of the sample, and SAM-modified areas of the sample. CdS deposition was generally restricted to the surface of the LB film. **B.** An atomic force micrograph (force mode imaging) of a region similar to that shown in Fig. 7A. **C.** An atomic force micrograph (force mode imaging, higher magnification than 7B) of the surface of the CdS film formed on the 5 layer LB film.

4. Conclusions

We have devised a method for template-assisted electrochemical deposition of CdS that produced adherent, conformal thin films with relatively fast deposition rates when compared to other solution precipitation methods. The methods described may form a route to the deposition of crystalline, uniform, thin CdS films that exhibit crystallographic orientations that are dictated by an underlying organic template where nucleation occurs.

Work is ongoing in our group to examine the mechanisms of deposition for the formation of such films. Emphasis in this work includes the investigation of possible cooperative assembly between the LB templates and the nucleated CdS crystals, and the effects of electric fields on the crystallization process. In addition, we are continuing to characterize the structures of CdS films deposited in this manner. Current efforts include analysis by transmission electron microscopy, X-ray diffraction and atomic force microscopy.

5. Acknowledgments

This work was supported in part by the National Science Foundation (HRD-9450475) and by the United States Department of Energy under Contract DE-AC04-94AL85000. Sandia is a multiprogram laboratory operated by Sandia Corporation, a Lockheed Martin Company, for the United States Department of Energy.

6. References

1 P. C. Rieke, S. B. Bentjen, *Chem. Mater.*, *5* (1993) 43.
2 Y. Fainman, J. Ma, S. H. Lee, *Mater. Sci. Rep.*, *9* (1993) 53.
3 T. L. Chu, S. S. Chu, N. Schultz, C. Wang, C. Q. Wu, *J. Electrochem. Soc.*, *139* (1992) 2443.
4 K. I. Grancharova, J. G. Bistrev, L. J. Bedikjan, G. B. Spasova, *J. Mater. Sci. Lett.*, *12* (1993) 852.
5 C. Trager-Cowan, P. J. Parbrook, F. Yang, X. Chen, B. Henderson, K. P. O'Donnell, B. Cockayne, P. J. Wright, *J. Cryst. Growth*, *117* (1992) 532.
6 T. Miyasato, M. Tonouchi, *Mater. Sci. Eng.*, *B9* (1991) 195.
7 E. Fatas, P. Herrasti, F. Arjona, E. G. Camarero, *J. Electrochem. Soc.*, *11* (1987) 2799.
8 B. R. Heywood, S. Mann, *Adv. Mater.*, *6* (1994) 9.
9 E. M. Landau, S. G. Wolf, M. Levanon, L. Leiserowitz, M. Lahav, J. Sagiv, *J. Am. Chem. Soc.*, *111* (1989) 1436.
10 Y. Tian, J. H. Fendler, *Chem. Mater.*, *8* (1996) 969.

11 R. S. Urquhart, C. L. Hoffmann, D. N. Furlong, N. J. Geddes, J. F. Rabolt, F. Grieser, *J. Phys. Chem.*, *99* (1995) 15987.
12 P. Facci, V. Erokhin, A. Tronin, C. Nicolini, *J. Phys. Chem.*, *98* (1994) 13323.
13 A. Ulman, *An introduction to ultrathin organic films : from Langmuir-Blodgett to self-assembly*, Boston, Academic Press, 1991
14 L. H. DuBois, R. G. Nuzzo, *Ann. Rev. Phys. Chem.*, *43* (1992) 437.
15 Digital Instruments, *Nanoscope II Scanning Probe Microscope Instruction Manual*, Ver. 5, Digital Instruments, Santa Barbara (CA), 1990.
16 N. Razik, *J. Mater. Sci. Lett.*, *6* (1987) 1443.
17 V. Skita, M. Filipkowski, A. F. Garito, J. K. Blaisie, *Phy. Rev.*, *B34* (1986) 5826.
18 S. Mann, B. R. Heywood, S. Rajam, R. J. Davey, J. D. Birchall, *Nature*, *334* (1988) 692.

APPENDIX C

Characterization of Langmuir - Blodgett Films Using X-ray Reflectivity

J. Cesarano, D. Chen, M. Kent, D. Fein

Materials and Process Science Center
Sandia National Laboratories

SUMMARY

X-ray reflectivity is a technique that measures the intensity of scattered x-rays that have been reflected from a surface at very small angles. This technique is very useful for determining the detailed structure of thin molecular films. However, there are limitations of this technique: 1) the structural information that is gleaned from this technique is primarily for structure throughout the thickness of the films. That is, the out-of-plane structure that is perpendicular to the substrate; 2) the structural information yields averaged information for the entire analysis area; and 3) The film structure does not come directly from the reflectivity data. An end user must guess what the actual structure may be and then use a model to calculate a reflectivity curve. If the calculated values fit the experimental data then it is assumed that the guessed structure is the actual structure. This may not be totally satisfying in that you may never be absolutely certain that there is a unique structural solution. However, in reality, the probability of having several solutions to one reflectivity curve is very low. In order to fit a reflectivity curve, four parameters must be used for each uniform layer within the structure and calculated curves vary greatly as each parameter is varied. The variables are thickness, roughness, and two parameters related to how the layer scatters x-rays.

The work described below is for the study of Langmuir Blodgett (LB) films of Cd-arachidate on silicon wafers. Cd-arachidate films up to 10 layers were analyzed. The structure of the LB films is actually comprised of several layered components. The silicon wafers have a native oxide layer that is 15Å thick. The native oxide is then rendered hydrophobic by chemically attaching a self assembled monolayer of octadecyltrichlorosilane. The Cd-arachidate LB films are then applied. For detailed analysis, each layer within the structure must be analyzed sequentially. The structure of the 15Å thick native silicon oxide had to be determined first. Then, the oxide/silane together and then the oxide/silane/LB structures. Details of this work are presented in the tables and Figures below. The main contribution of this work is that it was determined that knowing the scattering information for a single molecular species was not enough to fit the reflectivity data. Individual segments within molecules had to be accounted for. With that completed, relatively good fits were obtained and detailed information for the out-of-plane structure of Cd-arachidate on silicon was derived. In order to obtain a detailed model of the LB film, including in-plane structure, x-ray reflectivity should be coupled with other characterization techniques.

X-ray Reflectivity

- Detects the variation in the electron density of the specimen
- Has excellent resolution (~1nm)
- Is non-destructive
- Is ideal for use with thin samples such as Langmuir-Blodgett films
- The main drawback is that fitting the data is a lengthy process

1

X-ray Reflectometer

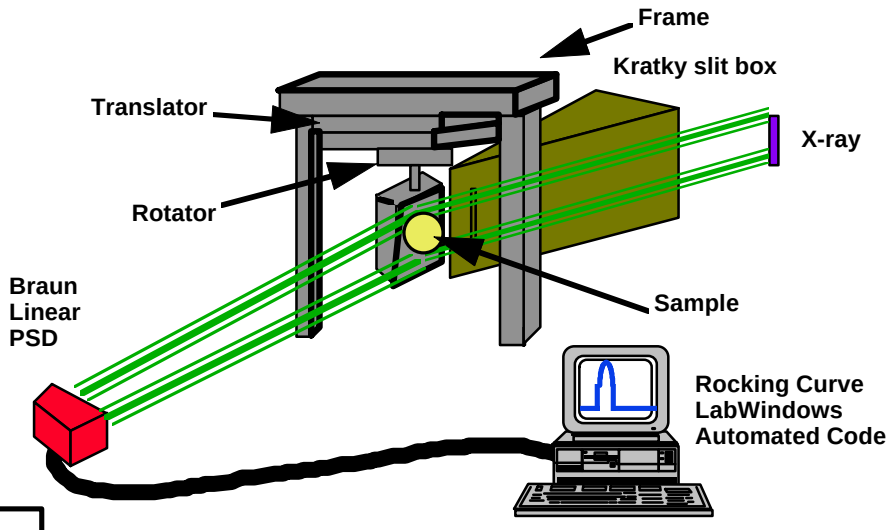

2

Calculating Reflectivity

- In vacuum, the z component of the wavevector is given by:

$$k_{z,0} = \left(\frac{2\pi}{\lambda}\right) \sin\theta = Q/2$$

- In a medium i, it is given by:

$$k_{z,i} = (k_{z,0}^2 - 4\pi\rho_i)^{1/2}$$

3

Reflectivity of a Simple Uniform Film

- The reflectance is given by:

$$r_{i,i+1} = (k_{z,i} - k_{z,i+1})/(k_{z,i} + k_{z,i+1})$$

- And the reflectivity is given by:

$$R(k_{z,0}) = \frac{r_{0,1}^2 + r_{1,2}^2 + 2r_{0,1}r_{1,2}\cos(2k_{z,1}d)}{1 + r_{0,1}^2 r_{1,2}^2 + 2r_{0,1}r_{1,2}\cos(2k_{z,1}d)}$$

4

Diagram of X-ray Path

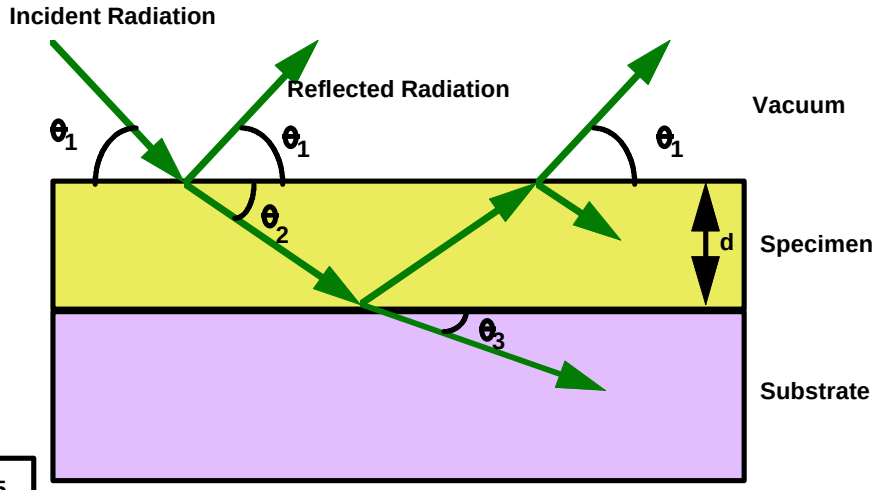

5

For Multiple Layer Reflectivity

- The x-ray is refracted, so the incident angle is different for lower layers.
- Using Snell's Law:

$$n_1 \cos\theta_1 = n_2 \cos\theta_2$$

n = Refractive index

$$n=1-Ž+iß$$

6

Calculation of Ž and ß

$$Ž = \frac{\lambda^2 p_{el} r_0}{2š}$$

λ = the wavelength of incident radiation
p_{el} = the electron density
r_0 = the classical electron radius

$$ß = \frac{\mu\lambda}{4š}$$

μ = the mass absorption coefficient

7

Roughness

- Roughness on a surface effectively makes the incident angle variable. This is accounted for in the theoretical calculations.

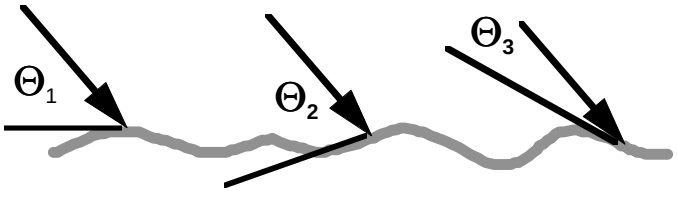

8

Experimantal

Preparation of Substrate(Silanation)

1) Rinse off substrate with Ethanol and DI water
2) Blow substrate dry
3) Rinse out Silanation bottles with Ethanol
4) Plasma clean substrate in Technics MICRO PD series 900 Plasma Cleaner
    a) Plasma clean for about 10 to 15 min
    b) Keep at 0.250 torr and about 40 watts
5) Transfer substrate and all materials into (N_2)dry box
6) Using syringes, transfer 20ml of hexadecane into each bottle
7) Add 8µl of Octadecyltrichlorosilane(OTS) to one of the bottles
    (concentration of OTS should be 1mM)
8) Transfer the substrate into the bottle with the silane-hexadecane mixture
    (substrate must be submerged in solution)
9) Let the reaction take place for approximately 2-4 hours
10) After the desired reaction time, transfer the substrate from the reaction mixture to the vial containing only hexadecane
11) Transfer everything out of the dry box
12) Take the sample out of the vial and rinse with Chloroform, Ethanol, and DI water. Scrub with a swab soaked in chloroform if necessary
13) Blow off sample with N_2 of Ar, and store in fluoroware or plastic box
14) Dispose of waste properly

Preparation of Flask that will contain subphase(Piranha Cleaning)

1) Wear full protective clothing(long rubber apron, face mask, appropriate gloves, long pants, and shoes
2) Carefully pour 4 volumes of Sulfuric Acid into the flask
3) Slowly pour 1 volume of 30% concentrated Hydrogen Peroxide into the acid
4) While pouring the H_2O_2, gas bubbles should start to form. BE CAREFUL! This reaction is very exothermic. Be careful when you place the cap on the flask. Do not keep the cap on for a long period of time. The gas that is formed must be allowed to exit the bottle. Failure to remove the cap fast enough may result in the bottle exploding due to gas pressure
5) Place the cap on, shake the bottle, and quickly remove the cap. Repeat this for at least 15 minutes. The reaction will slow down after a while, becoming less exothermic.
6) Pour the "Pirhana solution" into the appropriate waste bottle
7) Rinse the bottle with DI water straight from the faucet for at least 5 minutes
8) The bottle is clean when the bubbles that form from shaking the bottle disappear from the water. If the bubbles stay on the surface, then the bottle still contains organic ontaminants. The bottle can be used for the next 6 months without recleaning

Preparation of Subphase

1) Rinse out 2000ml flask with DI water straight from faucet
2) Measure out 0.1800g of $CdCl_2$(for a Cadmium concentration of $5x10^{-4}$M)and place in the empty flask
3) Fill the flask to the top(2000ml) with DI water
4) Shake until the $CdCl_2$ is dissolved and mixed thoroughly
5) Take pH of mixture
6) Adjust pH by adding 0.1M $NaHCO_3$ until the pH is about 6.50

Using the Nima Langmuir-Blodgett Trough

Preparation of the Trough

1) The surface of the trough, and all the parts of the trough which will be in contact with the subphase should be wiped with a Kimwipe soaked in isopropanol(wearing polyethylene gloves)
2) The trough should now be wiped with a Kimwipe soaked in DI water
3) The barriers should be attached, with the end of the barrier touching the outside edge of the trough
4) The pressure sensor is then attached. Take an "S" hook, and hook it to the pressure sensor wire. Attach the long copper colored wire to the other end, and attach another "S" hook to the other end of the copper wire. Then attach the Wilhelmy plate to the other end of the "S" hook
5) The subphase should then be poured into the trough. The surface of the subphase should be about 1-2mm over the top of the edge of the trough

Cleaning the Subphase

1) Before the Wilhelmy plate is lowered into the subphase, the surface should be cleaned
   a) Turn on the aspirator pump
   b) Put the pipette head at the surface of the subphase to suck off any floating material
   c) Move the pipette around to cover the whole area between the barriers
2) Lower the Wilhelmy plate completely into the subphase and let it sit for a few minutes
3) Make sure the barriers are fully opened, and position the pressure sensor so that about two-thirds of it is submerged in the subphase
4) Zero the pressure sensor(press the [Z] button)
5) Lift the pressure sensor out of the subphase. The pressure should change about 70mN/m(the exact value for pure water in an atmosphere of saturated water vapor at 293K is 72.8mN/m)
6) Reposition and rezero the sensor
7) Press the [ENTER] button to start the isotherm. The isotherm should be constant except for a small peak at the end, caused by contaminants on the subphase surface
8) Suck off the surface of the subphase again, and open the barriers
9) Repeat steps 8 and 7 and 8 until the pressure(^{1}a) is less than 0.5mN/m when the barriers are closed
10) If the subphase level is too low, pour more in until the level is high enough
11) Check the pressure again
12) Open the barriers completely

Spreading the Monolayer

1) Rinse out a 100µl syringe with chloroform about 3 times
2) Get about 100µl of Arachidic Acid in Chloroform(2mM ~ 25mg/40ml)
3) Hold the syringe tip about 5-10 mm from the surface of the subphase
4) Place one drop of the Arachidic Acid on the surface of the subphase
5) Wait for the drop to completely disappear, and repeat until all 100µl are deposited on the surface
6) Repeat steps 2 through 5 until about 300µl of the Arachidic Acid solution is deposited on the surface
7) Let the chloroform evaporate for at least 15 minutes.

Dipping the Sample

1) Place the substrate in the holder, and place the holder on the trough
2) Lower the substrate until it is very close to the surface of the subphase
    a) Press [D] to move the dipper
    b) Press [D] again to tell the dipper to go down
    c) Let the dipper lower
    d)Press [SPACE BAR] to stop the dipper
3) Program the dipper
    a) Press [M] to go to the menu
    b) Program dipping conditions
        1: Press [D] to go to the dipper menu
        2: Press [A] to set the area of the substrate
        3: Press [N] to set the number of layers to be dipped
        4: Press [T] to set the target pressure (28mN/m)
        5: Press [D] to set the dipping speed (1.6mm/min)
        6: Press [W] to set the dipper wait (Use ~60s)
            A) This tells the dipper what duration to wait between each bilayer
    B) If no wait is desired, leave it at 0s
        7: Set dipper start and end
            A) Press [E] to switch from enter to teach mode
            B) Press [1], and the location of the dipper currently will appear
                1- Press [SPACE BAR]
                2- Press [Y] to log the position as the start position
            C) Press [E] to switch back to enter mode
            D) Press [2] and enter the end position
        8: Press [Q] to exit dipping menu
    c) Program operating conditions
        1: Press [V] and enter the volume of Arachidic Acid solution used
        2: Press [B] to change barrier speed
        3: Add any comments
        4: Press [Q] to exit the operating conditions menu
    d) Press [Q] to return to the isotherm
4) Cover the trough opening with the plastic sheet
5) Zero the pressure sensor(Press [Z])
6) Press [ENTER] to start the compression of the monolayer
7) When the pressure is close to the target pressure, hit [SPACE BAR]
8) Press [P] to turn on the pressure control, and press [ENTER] to compress the barriers
9) When the target pressure is reached, hit [D] to begin the dipping program
10) When the dipping is done, raise the dipper all the way
11) Remove the holder, and remove the sample. Place the sample in a plastic sample box
12) Press [S] to save data

Emptying the Trough

1) Open the barriers completely (Press [O])
2) Plug in the aspirator pump
3) Suck off the surface of the subphase
4) Press [E] to begin easy clean
    a) The barriers will compress to the target pressure, and the
5) Suck out all the subphase
6) Remove the pressure sensor, and the barriers
7) Wipe the surface with kimwipes soaked in isopropanol and DI water
8) Put on trough cover and close doors
9) Press [Q] to quit the trough program
10) Turn off the computer and the trough

Sample conditions for figures

Fig. 9 Si/SiO_2 15Å
Rinsed with Ethanol and DI water
Plasma Cleaned
Substrate dimensions = 1'x1'

Fig. 10 Si/SiO_2 15Å with 1 layer of Octadecyltrichlorosilane
Rinsed with Ethanol and DI water
Plasma Cleaned
Silanated in 25ml of hexadecane and 10µl of OTS for 4 hours
Scrubbed with a swab soaked in Chloroform
Rinsed with Chloroform, Ethanol, and DI water
Substrate dimensions = 1'x1'

Fig. 11 Si/SiO_2 15Å with 1 layer of OTS and a 2 layer LB film of cadmium arachidate
Rinsed with Ethanol and DI water
Plasma Cleaned
Silanated in 20ml of hexadecane and 8µl of OTS for 4 hours
Scrubbed with a swab soaked in Chloroform
Rinsed with Chloroform, Ethanol, and DI water
Dipped diagonally using alligator clip holding the corner
Subphase conditions - 0.180g $CdCl_2$, adding ~1.5ml of

0.1M $NaHCO_3$ pH = 6.49 $[Cd^{++}] = 5x10^{-4}M$

Dipper speed = 1.6 mm/min
Target pressure = 28mN/m
Barrier Speed = 50cm^2/min
285µl of Arachidic Acid/Chloroform solution(2mM) deposited on surface
Dipper wait = 0 seconds
Dipper start position = 24.6mm
Dipper end position = 55.0mm
Length of film ~ 30.0mm
Substrate dimensions = 1'x1'

Fig. 13 Si/SiO_2 15Å with 1 layer of OTS and a 10 layer LB film of Cd-arachidate
Rinsed with Ethanol and DI water
Plasma leaned
Silanated in 30ml of hexadecane and 12µl of OTS for 4 hours
Scrubbed with a swab soaked in Chloroform
Rinsed with Chloroform, Ethanol, and DI water
Subphase conditions - 0.180g $CdCl_2$, adding ~1.5ml of

0.1M $NaHCO_3$ pH = 6.53 $[Cd^{++}] = 5x10^{-4}M$

Dipper speed = 1.6 mm/min
Target pressure = 28mN/m
Barrier Speed = 50cm^2/min
285µl of Arachidic Acid/Chloroform solution(2mM) deposited on surface
Dipper wait = 60 seconds
Dipper start position = 40mm
Dipper end position = 74mm
Length of film ~ 34mm
Substrate dimensions = 1'x1.5'

Thickness Å	Delta	Beta	Roughness Å	
0	7.4	0.173	3	silicon substrate
15	7.5	0.098	4	silica

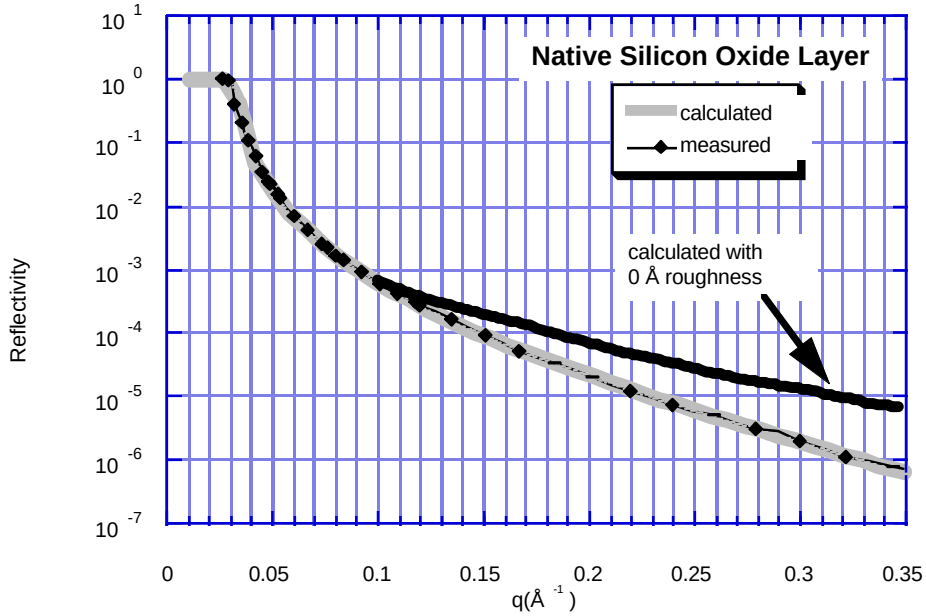

Figure 9: Reflectivity data and fit show that the native oxide layer on our silicon wafers is 15Å thick with a roughness of 4Å. A roughness value 4Å was necessary to obtain a good fit with the experimaental data

Th. (Å)	Delta x10 $^{-6}$	Beta x10 $^{-6}$	R (Å)	
0	7.5	.173	3	silicon substrate
15	7.5	.098	4	silica
5.5	4.22	.1585	1	silane head groups
15.2	3.48	.00431	5	hydrocarbon tail
1.0	.445	.00004	0	silane H group

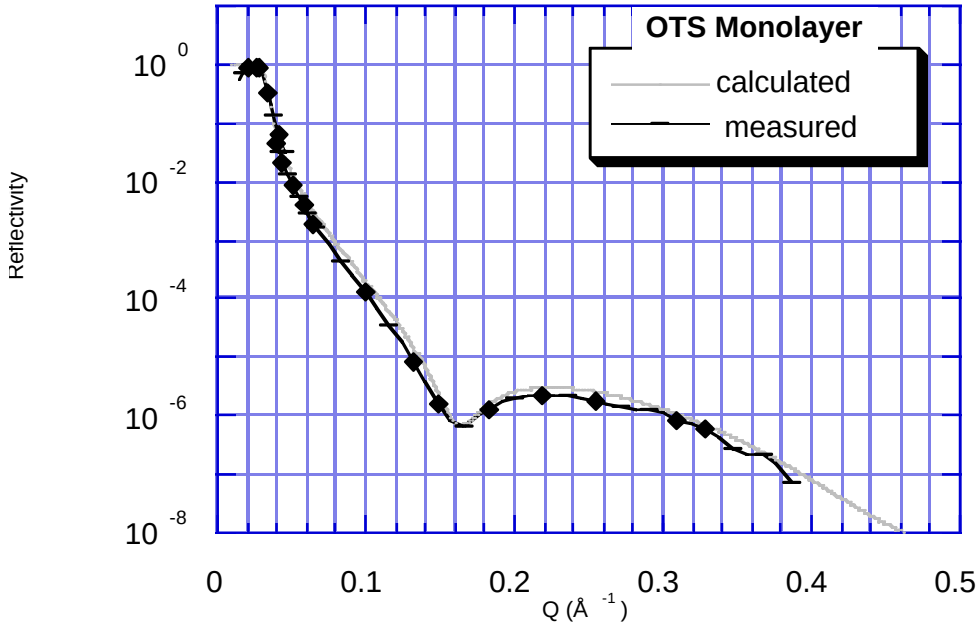

Figure 10: This reflectivity data and fit show that the OTS monolayer is conformal to the substrate with a roughness of 5Å. Also, this fit shows that OTS molecules need to be anaylzed as three entities

Th. (Å)	Delta x10 $^{-6}$	Beta x10 $^{-6}$	R (Å)	
1.2	.97	.01	.2	silane-arachidic (H-H)
24.1	3.48	.00431	3	arachidic hydrocarbon tail
4.4	10.72	.5443	.4	head groups (COO-Cd-OOC)
24.1	3.48	.00431	3	arachidic hydrocarbon tail
.6	.445	.00004	.1	arachidic tail (H)

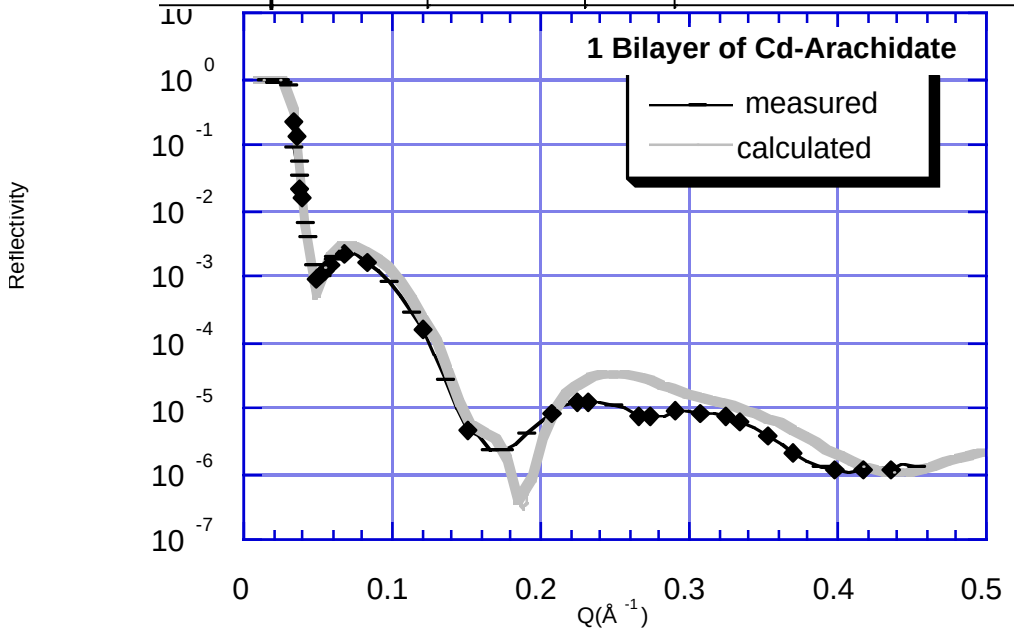

Figure 11: Reflectivity for one LB bilayer of Cd-arachidate. The fit is reasonable and shows that the bilayer is tilted about 15 degrees (see Figure 12). However the calculated structure shows more detail than the actual structure and implies that the bilayer is not as ordered as depicted in Figure 12

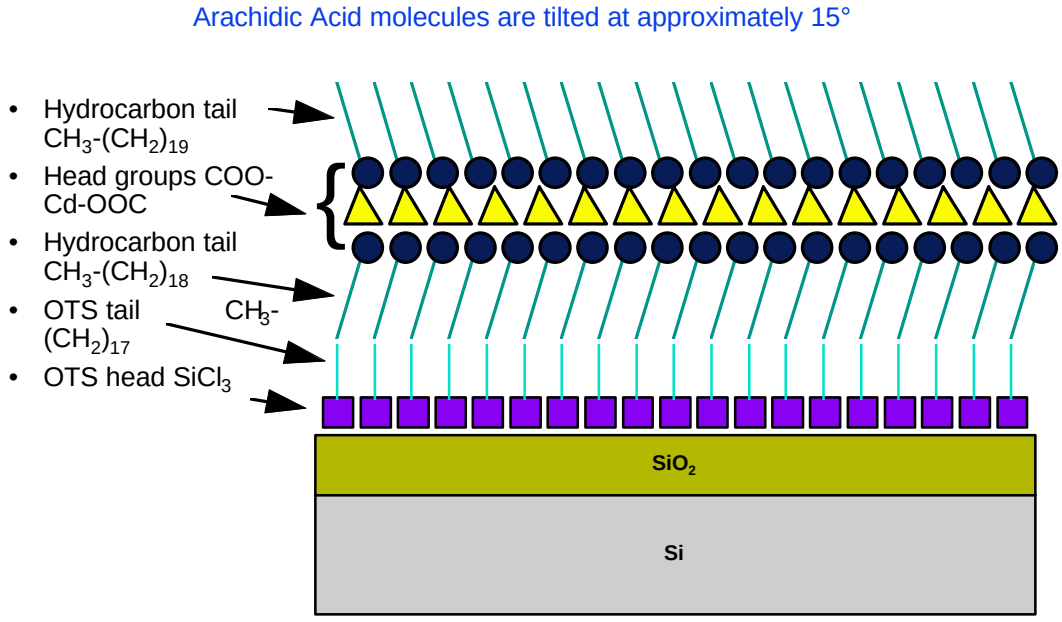

Figure 12: A schematic of the structure that was used to fit the data in Fig. 11. This fit shows that the Cd head group region must be treated separately from the rest of the bilayer. Also, the length of the hydrocarbon tails used to fit the data (24.1 Å) implies that the tails are actually tilted approximately 15 degrees from vertical.

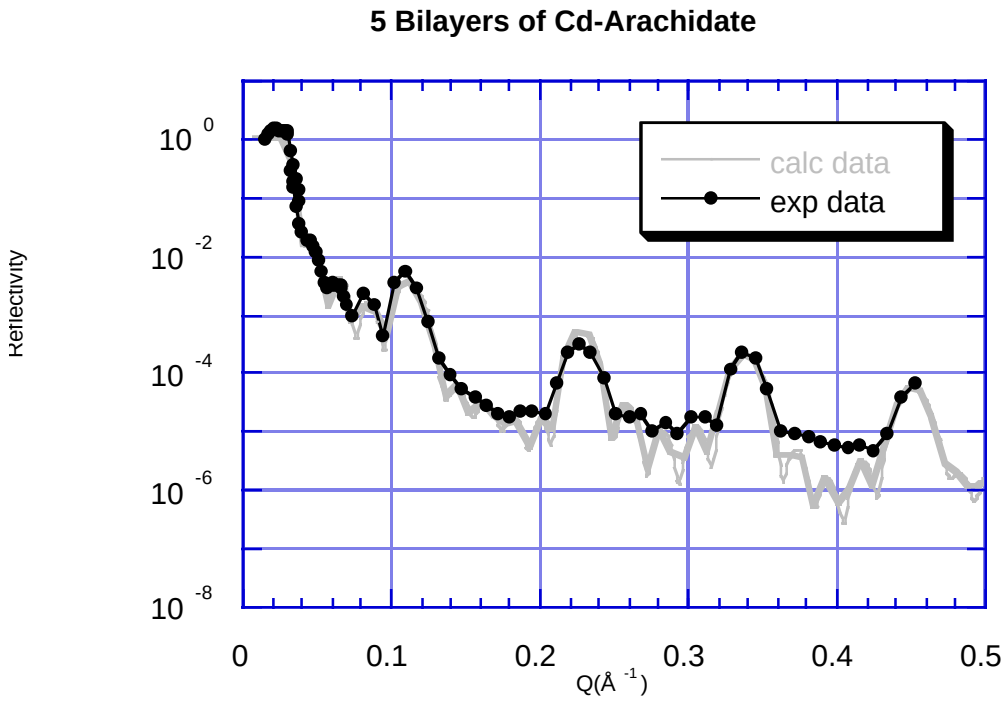

Figure 13: Reflectivity from 5 bilayers of Cd-arachidate. The actual structure does not have the very fine detail of the fitted model structure (see Fig. 14). However, the fit and hydrocarbon tail length, imply that the LB structure is a rigid crystalline structure that is not tilted. This may explain why 5 layer Cd-arachidate films provided better templating for CdS growth than the 3 layer Cd-arachidate films discussed in Appendix B.

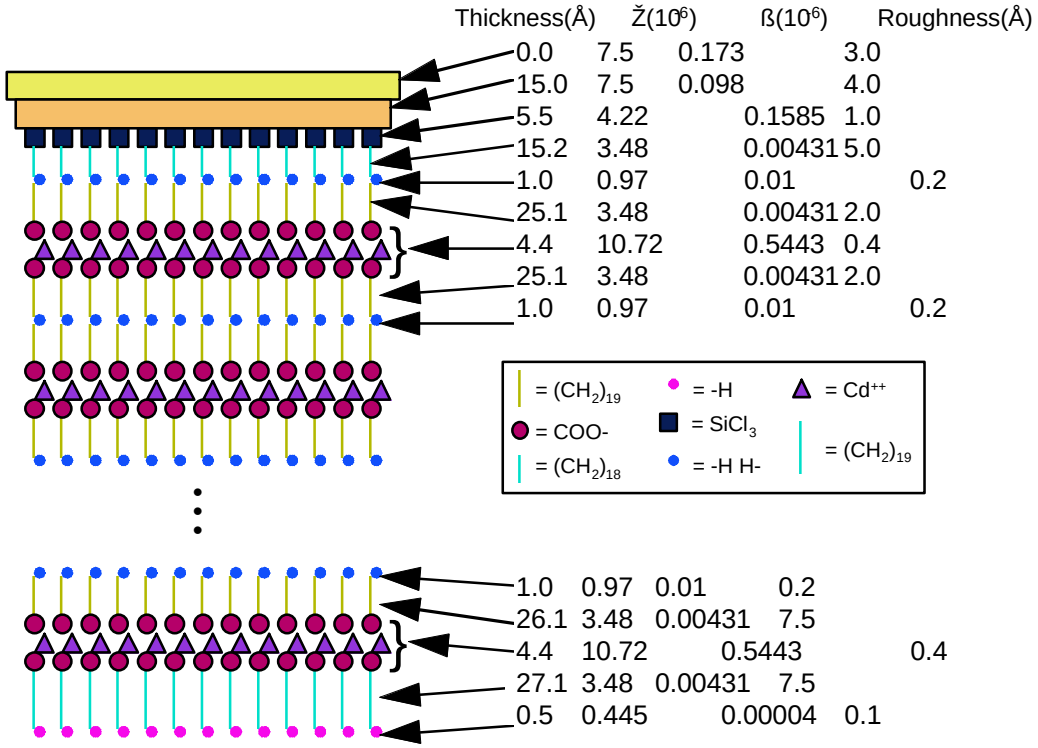

Figure 14: A schematic of the structure used to fit the reflectivity data in Fig. 13. The structure is not tilted with a bilayer thickness that is comparable to crystalline Cd-arachidate. The expected bilayer thickness for Cd-arachidate is approximateky 56Å. Bilayers #1-4 yield a thickness of 55.6Å +/- 1Å. Bilayer #5 yields a thickness of 58.6Å +/- 4Å

References

Russell, T.P. (1990) *"X-ray and neutron reflectivity for the investigation of polymers"* Materials Science Reports 5 pp.171-271

Stanglmeier, F., Lengeler, B., Weber, W., Gobel, H. & Schuster, M. (1992). *Acta Cryst.* A**48**, 626-639

DISTRIBUTION:

5	MS-1349	J. Cesarano
1	MS-1407	M. Kent
1	MS-1407	D. Fein
1	MS-0860	R. J. Simonson
1	MS-1411	D. Dimos
1	MS-0333	A. Hurd

1 Gabriel Lopez
Chem. & Nuc. Eng.
Ferris Eng. Center / Rm 209
University of New Mexico
Albuquerque, NM 87131

1	MS- 9018	Central Technical Files, 8940-2
5	MS-0899	Technical Library, 4916
2	MS-0619	Review & Approval Desk, 12690 For DOE/OSTI
1	MS-0161	Patent and Licensing Office, 11500